A Solution to the Braced Excavation Collapse in Singapore

By

Javier Artola

B.S., Civil Engineering
Stevens Institute of Technology, 2003

SUBMITTED TO THE DEPARTMENT OF CIVIL AND ENVIRONMENTAL ENGINEERING IN PARTIAL FULFILLMENT OF THE REQUIREMENTS FOR THE DEGREE OF

MASTER OF ENGINEERING IN CIVIL AND ENVIRONMENTAL ENGINEERING

AT THE
MASSACHUSETTS INSTITUTE OF TECHNOLOGY

JUNE 2005

Signature of Author _____
Department of Civil and Environmental Engineering
May 24, 2005

Certified by _____
Andrew J. Whittle
Professor of Civil and Environmental Engineering
Thesis Supervisor

Accepted by _____
Andrew J. Whittle
Chairman, Departmental Committee for Graduate Students

A Solution to the Braced Excavation Collapse in Singapore

By

Javier Artola

Submitted to the Department of Civil and Environmental Engineering
On May 24, 2005 in Partial Fulfillment of the Requirements for the Degree of
Master of Engineering in Civil and Environmental Engineering

ABSTRACT

At about 3:30pm on April 20, 2004, a 30m deep excavation adjacent to Nicoll Highway in Singapore collapsed, resulting in four casualties and a delay of part of a US$4.14 billion subway project. This thesis examines the flaws in the original design of the bracing system, which have been cited as causes of the failure. The Author then proposes a revised design for the braced excavation system.

The Plaxis finite element program was used to simulate the excavation process and compute forces on the major structural elements in the original design. Some pertinent background information on this program is provided throughout the thesis in order to better understand the significance of certain errors in the input data of the original model that ultimately led to the incorrect assumptions and calculations of the original design. A new model using this same program was regenerated with a corrected set of input assumptions, thereby leading to reasonable estimates of structural forces. These results were then used to propose a revised design of the excavation support system and compare this design to the original used in the excavation project. There are several lessons that could be learned from this structural failure, one being the need to acknowledge the limitations built in advanced analysis software systems, and another being the importance of ascertaining that the user understands every feature of the product.

A cost estimation of the proposed design is given and compared to the original design in order to evaluate the viability of the proposed design in the construction bid. Finally, some important conclusions are drawn from this study that should be applied to future large-scale construction projects where public safety and welfare is at stake.

Thesis Supervisor: Andrew J. Whittle
Title: Professor of Civil and Environmental Engineering

Acknowledgements

I would foremost like to thank my parents for their unwavering support of my interests and goals, in academia and elsewhere.

For this thesis, I owe a great deal to Professor Andrew Whittle, without him I would have never been exposed to this interesting research. His guidance and efforts encouraged me to find a solution to this problem and led me to the culmination of my thesis project.

Professor Jerome Connor has been a wonderful mentor and inspiration to me, and I would like to acknowledge his wisdom and support in every aspect of my life at MIT.

I would like to acknowledge Pat Dixon and Cynthia Stewart, for their support and patience in the submission of my thesis.

I would also like to acknowledge my dearest girlfriend, Wendy, for all her help and support and for being that joyful thought in the most stressful times.

Finally, I would like to acknowledge the families of the victims of this tragedy, may God be with you and your loved ones in the afterlife, and may their deaths serve as a remembrance of the commitment and responsibility that we – engineers – have *pro bono publico* (for the good of the public).

Table of Contents

Table of Figures

List of Tables

1. Introduction

Braced excavation systems are widely used in a variety of construction projects, such as cut-and-cover tunnels and building basements. Common malpractice or negligence in the design and construction of such systems can result in large-scale losses of capital and human lives. There are several examples of excavation collapses and corresponding studies that investigate their origins. This thesis examines one in particular: the 30m deep excavation collapse adjacent to Nicoll Highway in Singapore, which occurred on April 20, 2004. There have been various reports that explain the causes of this collapse. The final report of the Singaporean Ministry of Manpower (MOM) Committee of Inquiry has just been released, and is cited frequently throughout this thesis. However, it is not the author's intent to further analyze these studies, but instead to use the information already available to propose an alternate and effective design for the excavation system.

A finite element model using the soil-structure analysis program Plaxis v.8.0 was generated for this excavation using the proper parameters to obtain data on the required design capacities for the temporary diaphragm wall, strutting system, waler connection, and other elements of the project.

All the design procedures are explained in detail throughout this thesis. The original design was performed as per the British code BS8002 for soil-strut interaction and BS5950 for structural steel design. However, the proposed design was done using the American Association of State Highway and Transportation Officials (AASHTO) Standard Specifications for Highway Bridges (14^{th} Edition) and the American Institute of Steel Construction (AISC) Allowable Stress Design (ASD) Manual of Steel Construction (9^{th} Edition). The final design of the excavation system was obtained through an iteration process of the model and design criteria.

2. Review of Slurry (Diaphragm) Wall Excavation Systems

2.1 General Methods of Slurry Wall Construction

Slurry wall design and construction demands attention to a variety of factors such as slurry materials (i.e. processing), excavating equipment, and panel size. For example, the depth of the slurry wall may be determined by the soil conditions present at the site, or the site layout may limit panel sizes. One often encounters existing utilities or nearby buildings in urban excavations and they may need to be protected or relocated. In addition, water-stopping details should be given special consideration because slurry walls are frequently part of the permanent structure. Working schedules can also be impacted by the requirements for traffic maintenance. Construction procedures should therefore address these and other relevant issues in order to optimize the construction project as a whole.

A slurry wall is constructed by linking a series of slurry wall panels in a predetermined sequence. The panels are excavated to specified dimensions while at the same time slurry or another stabilizing fluid is circulated in the trench. Excavation equipment may range from simple clamshell buckets to hydraulic clamshells to hydrofraises (Xanthakos, 1994, Parkison & Gilbert, 1991, Ressi, 1999, Bauer, 2000). In addition, individual contractors have developed their own f(typically) patented trenching equipment. Figure 1 displays a variety of trenching equipment employed in slurry wall construction. (Konstantakos, 2000).

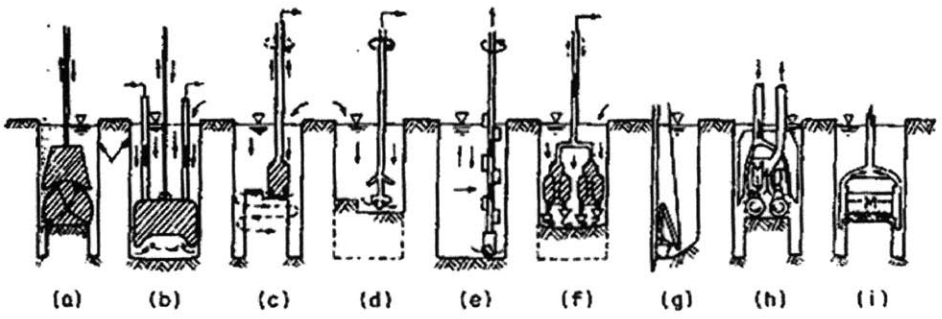

Figure 1: Trenching Equipment (Xanthakos, 1991)

(a) Clamshell bucket attached to a kelly. (b) Vertical percussive bit with reverse circulation, (c) Percussive benching bit. (d) Rotary benching bit. (e) Rotary bit with vertical cutter. (f) Rotary drilling machine with reverse circulation. (g) Bucket scraper. (h) Bell-mouth suction rotary cutter with direct circulation. (i) Horizontal auger machine.

Figure 2 presents the basic steps in typical slurry wall construction. The first step is to clear the site of any possible obstructions. Guide walls are then built to stabilize the upper few feet of soil and to guide the trenching equipment (controlling the vertical orientation of the panels). End-stops are inserted into the panel after trenching is completed in order to help form water-tight joints connecting adjacent panels. The end-stops are withdrawn after the adjacent panel is trenched.

After a panel is excavated to the specified dimensions, then a reinforcement cage is placed into the slurry filled trench. Reinforcement cages may be spliced if the required cages are too heavy for the lifting equipment.

The bottom of each panel is cleaned prior to concreting because sands and other soils may form intrusions that undermine the integrity of the wall (i.e. its water-tightness, stiffness, and strength). Concrete is then carefully tremied into the trench and continuously displaces the slurry therein. The top few inches of the panel are always chipped in order to bring the fresh concrete to the surface because the slurry is trapped in the top inches of the panel.

An important issue in the concreting process is the segregation of concrete aggregates during fast concreting. Slurry can become trapped within the tremied concrete, thereby creating soft zones within the slurry walls. If the panel bottom is not properly cleaned, then the soil and the waste that may have accumulated there may shift upwards during concreting as a result. This can lead to major leakage problems (Konstantakos, 2000). Successful construction depends upon careful construction to detail on site.

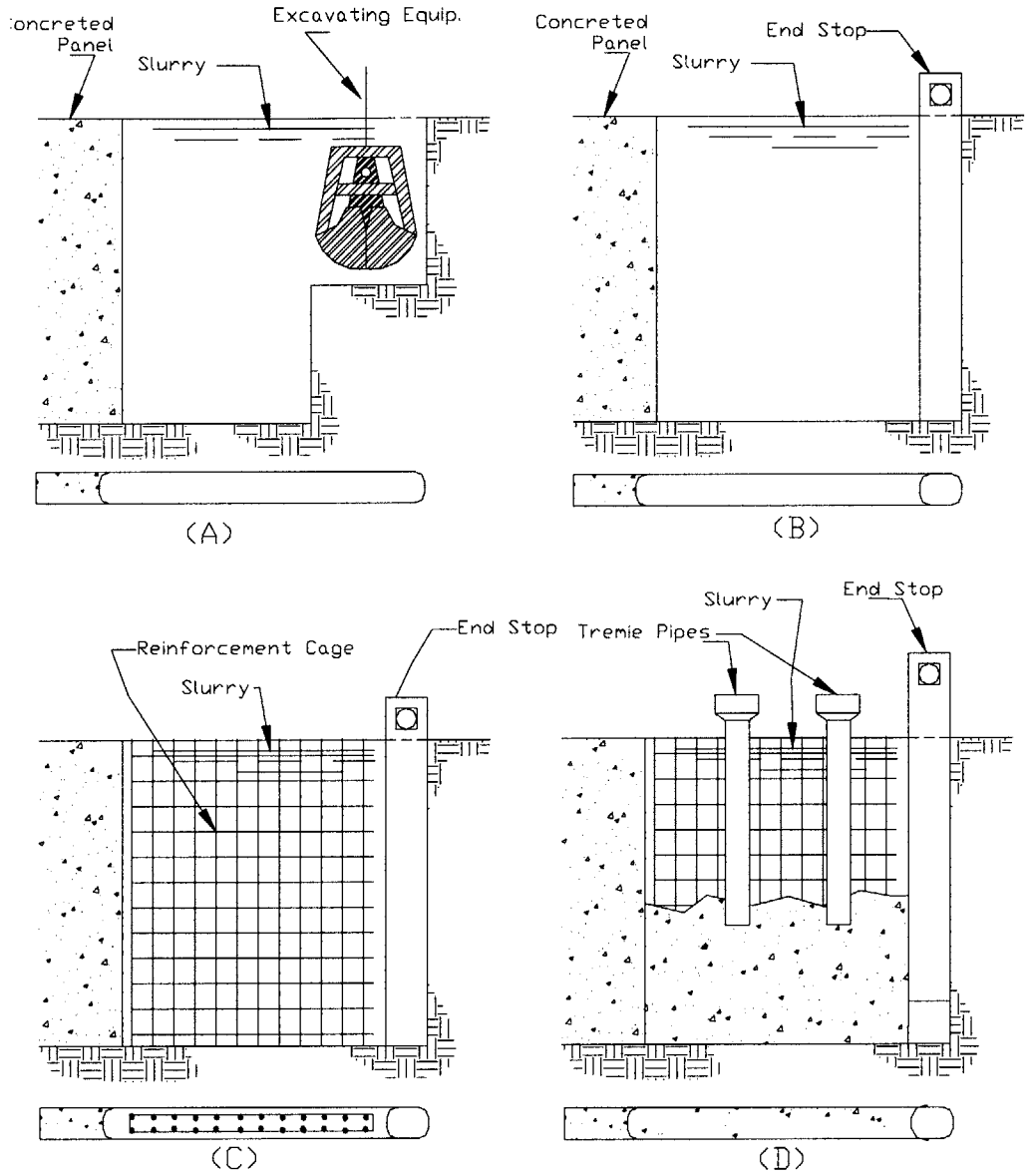

Figure 2: Typical Construction Sequence of Slurry Walls (Konstantakos, 2000)

(A) Trenching under slurry, (B) End stop inserted (steel tube or other), (C) Reinforcement cage lowered into the slurry-filled trench, (D) Concreting by tremie pipes.

2.2 Cross-Lot Braced Slurry Wall Excavations

Cross-lot bracing shifts the lateral earth (and water pressures) between opposing walls through compressive struts. The struts are usually either pipe or W-sections and are typically preloaded in order to produce a very stiff system. Installation of the cross-lot struts is accomplished by excavating soil locally around the strut and only continuing the excavation once preloading is finished. A typical sequence of excavation in cross-lot braced excavations is presented in Figure 3. The struts rest on a succession of wale beams that distribute the strut load to the diaphragm wall.

Pre-loading ensures rigid contact between interacting members and is achieved by placing a hydraulic jack as each side of an individual pipe strut between the wale beam and a special jacking plate welded to the strut (Fig. 4, Xanthakos, 1994). The strut load can be measured with strain gages or can be calculated using equations of elasticity by measuring the augmented separation between the wale and the strut.

When the struts were not preloaded in several previous projects, it resulted in large soil and wall movements as the excavation progressed downward. It has therefore become standard practice to preload the struts in order to minimize subsequent wall movements.

Cross-lot bracing is advisable in narrow excavations (18m to 36m) when tieback installation is impossible. The struts' serviceability can be adversely affected if the deflections at the struts are too large. This can occur when the struts' unbraced length is considerable, thereby causing the struts to bend excessively under their own weight if the excavation spacing is too great. Furthermore, special provisions should be to taken in order to account for possible thermal expansion and contraction of the struts (Konstantakos, 2000).

The typical strut spacing is approximately 5.0m in both the vertical and the horizontal direction. This is larger than the customary spacing when tiebacks are used because the pre-loading levels are much greater. A clear advantage of using struts is that there are no tieback openings in the slurry wall, thereby eliminating one source of potential leakage.

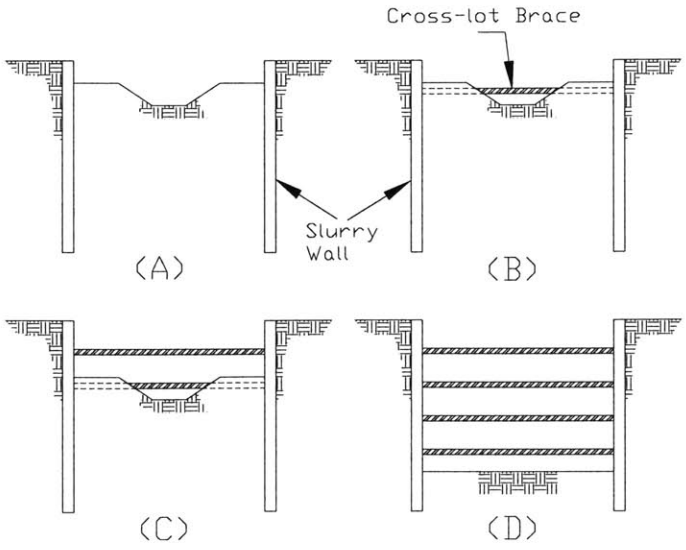

Figure 3: Typical Excavation Sequence in Cross-lot Excavations

(A) V-cut initial cantilever excavation, (B) Strut installation and pre-loading in small trenches in soil berms, (C) V-cut excavation to next level and strut installation, (B) Final grade.

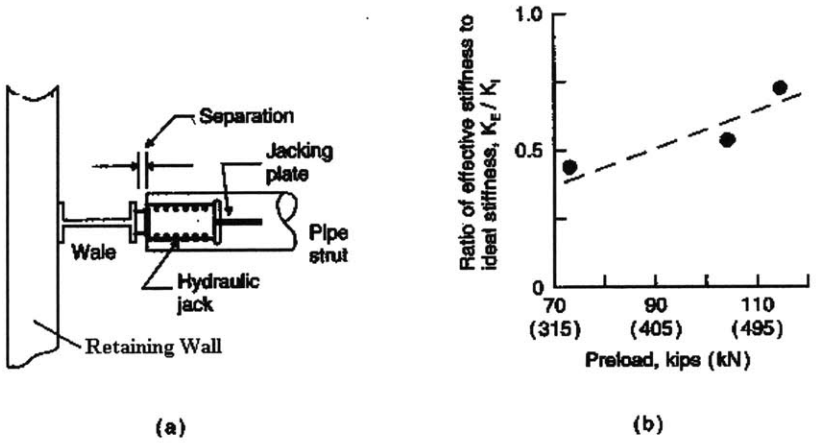

Figure 4: (a) Preloading Arrangement, and (b) Measured Brace Stiffness (Xanthakos, 1994)

3. The Original Design

3.1 Overview of the Project

The original excavation design was part of an ongoing 33.6 km Circle Line (CCL) subway project for Singapore's Mass Rapid Transit System that was set to be completed in 2009. With a cost of approximately US$4.14 billion, the entire CCL project will be a fully underground orbital line linking all radial lines leading to the city and will be completed in 5 stages (Figure 5).

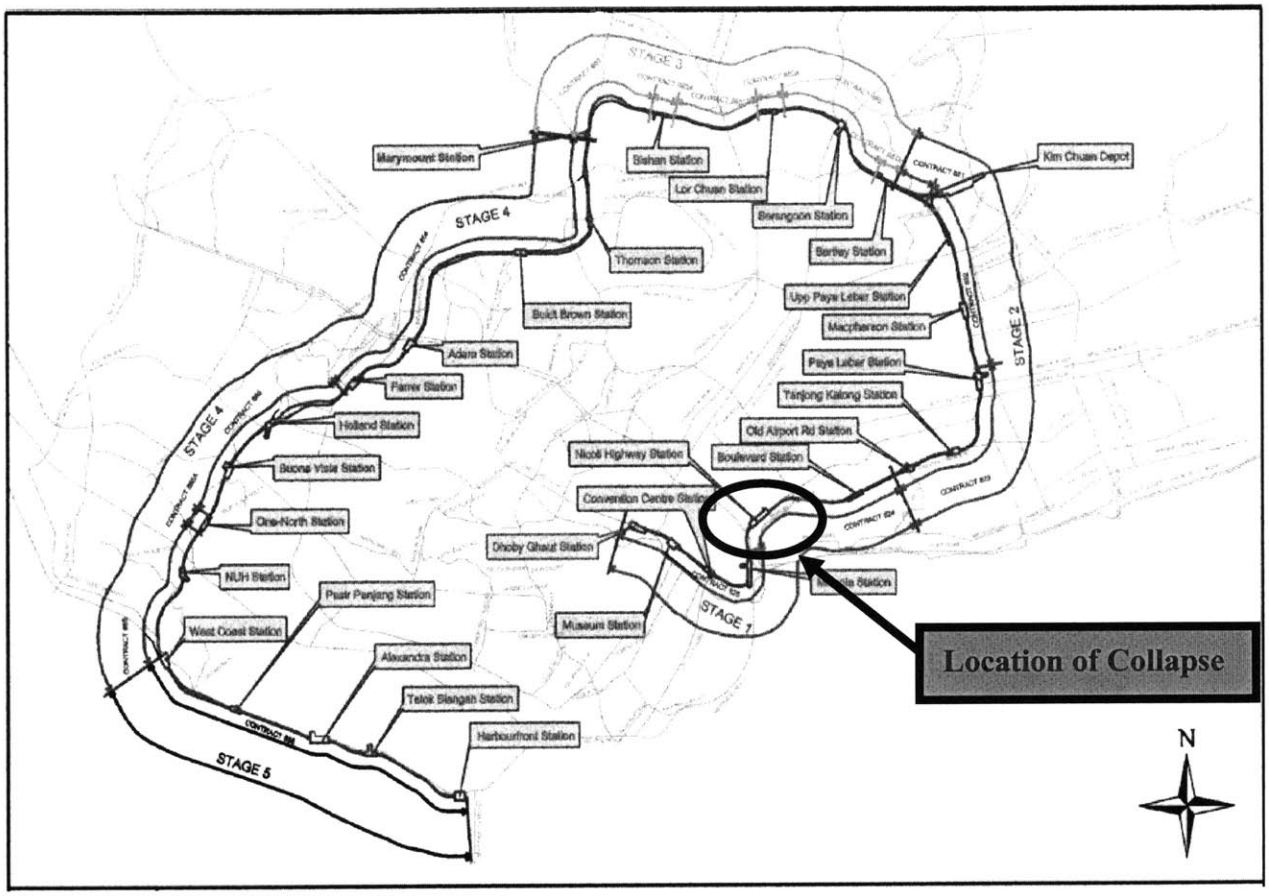

Figure 5: Overview of Circle Line Construction Stages 1 to 5 (MOM, 2005)

The excavation where the collapse occurred was part of a cut and cover tunneling project that was being done adjacent to Nicoll Highway in Stage 1 of construction (Figure 6). The route length covered by this contract was approximately 2.8 km. The temporary works to construct the cut and cover tunnel used diaphragm walls to support the sides of the excavation, steel struts to

brace these walls, and jet grout slabs constructed using interlocking Jet Grout Piles (JGP). Further explanation on these members will be provided in the following sections of the thesis.

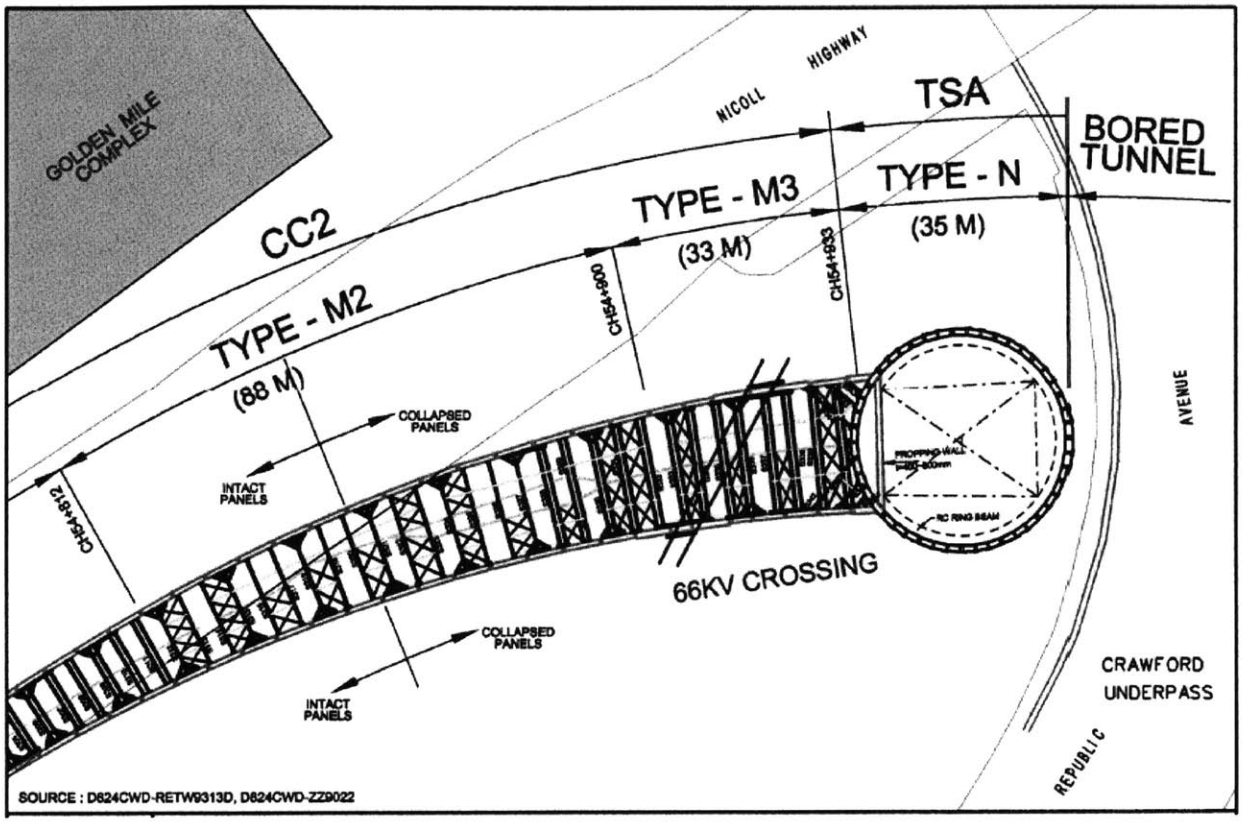

Figure 6: Overview of Cut and Cover Tunnel Adjacent to Nicoll Highway (MOM, 2005)

The accident area in which the collapse occurred was primarily centered at the Type M2 and Type M3 areas. The Type M3 area is the critical part of the excavation requiring particular focus (Figure 7). This area is comprised by 12 panels (6 on the north wall and 6 on the south wall). The wall panels were mostly 0.8m thick. The total length of the Type M3 area is about 33m. The design depth of the walls varied between 38.1m to 43.2m.

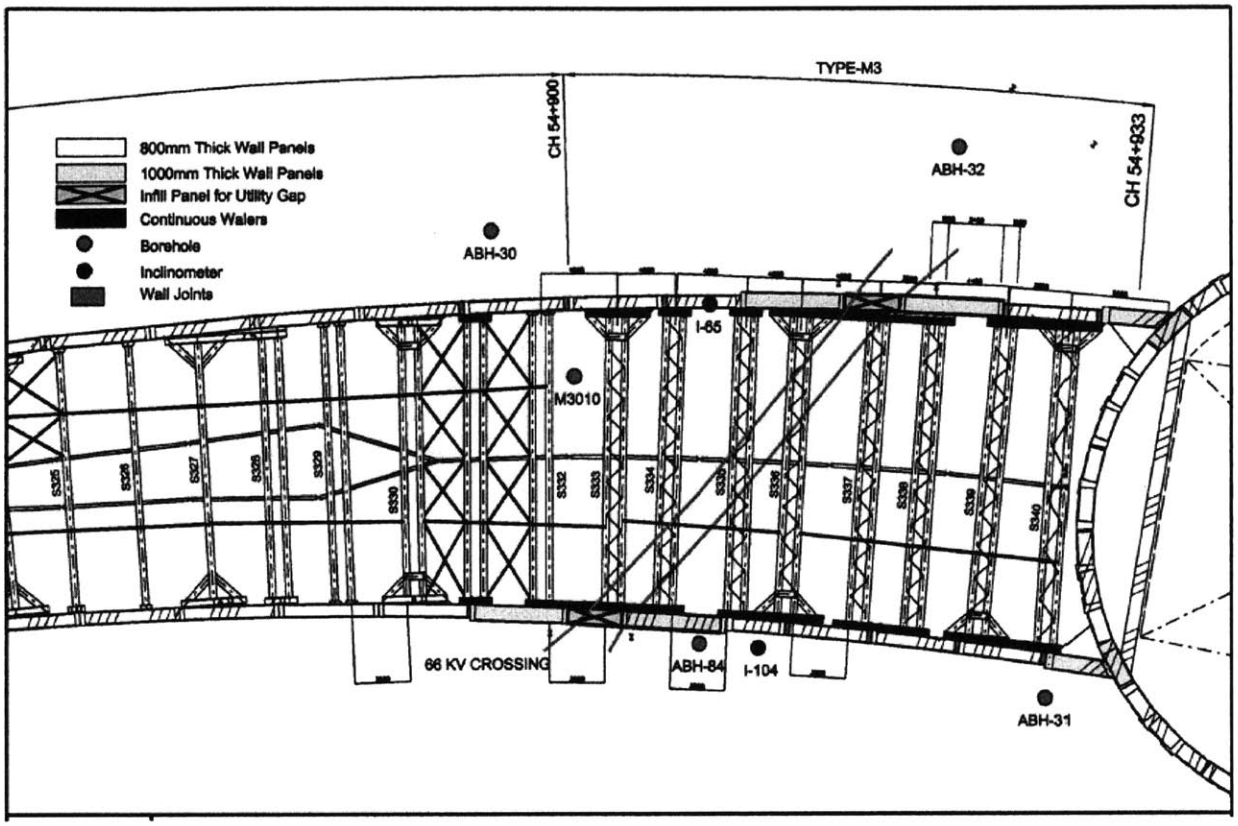

Figure 7: Overview of M3 Area (MOM, 2005)

3.2 Design of M3 Support System

Figure 8 summarizes the assumed soil stratigraphy for the M3 section together with the design of the lateral earth support system and location of the final tunnel boxes. The initial cut-and-cover excavation was approximately 20m wide and reached a maximum depth of 33.3m. The excavation was supported by 10 levels of cross-lot struts. These struts were supported by a central line of kingposts (Fig. 5 and Fig. 6) that extend deep into the first layer of the Old Alluvium (SW2). Two layers of interlocking Jet Grout Piling (JGP), 1.5m and 2.6m thick, were pre-installed to control ground deformations and reduce bending moments in the perimeter diaphragm wall panels. The upper JGP is a sacrificial layer that is removed during the excavation process. The final tunnel boxes are supported on drilled shafts (each 1.6m diameter) that extend into the fundamental Old Alluvium (CZ).

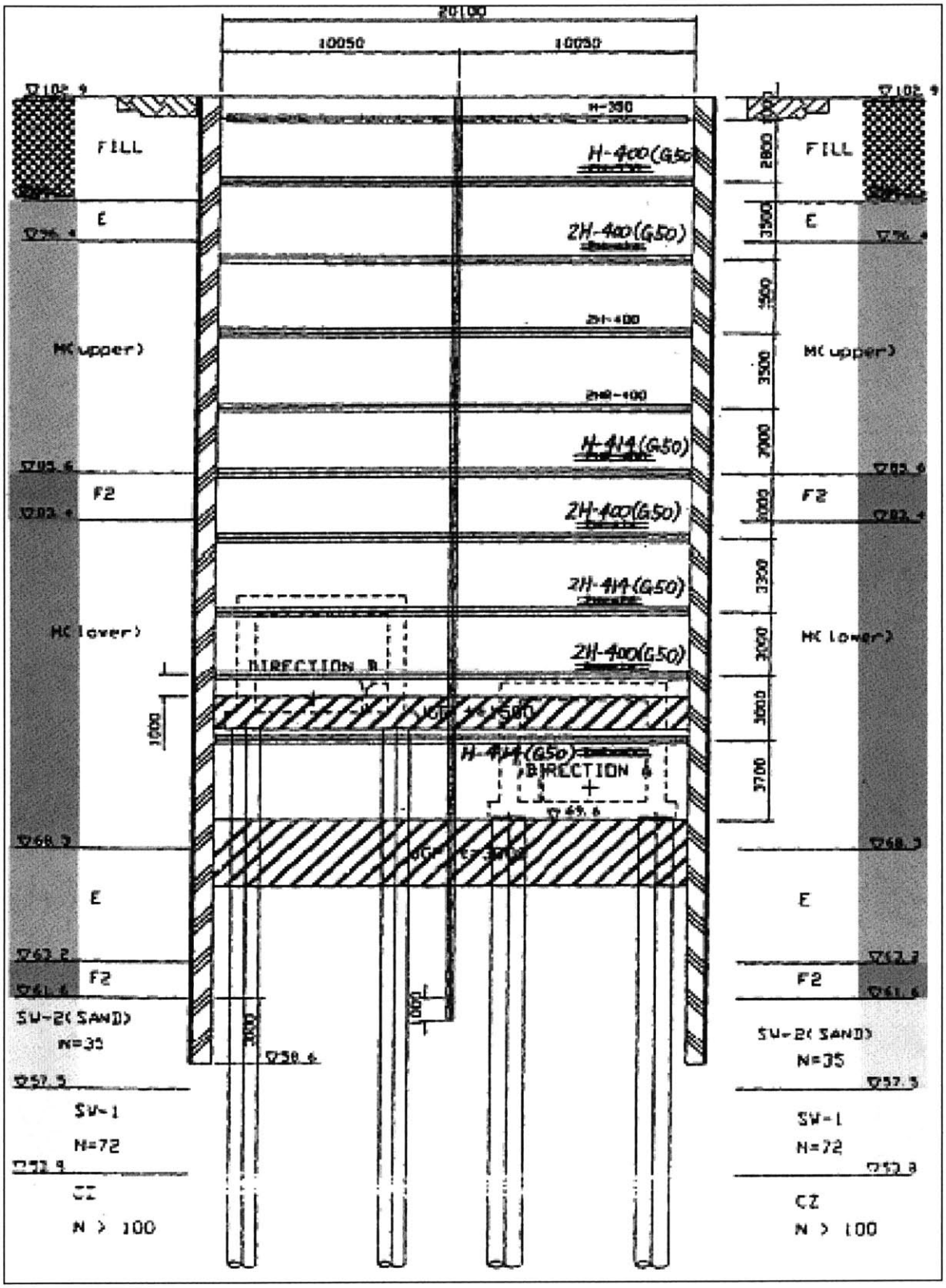

Figure 8: Soil Profile and Design Support System for M3 Section (MOM, 2005)

Fill		
Kallang Formation	Upper Estuarine (E)	Peats and organic soft clays (discontinuous)
	Upper Marine Clay M)	very soft clay
	Fluvial Sand (F1)	predominantly loose sand (discontinuous)
	Fluvial Clay (F2)	mainly firm clays (discontinuous)
	Lower Marine Clay (M)	soft clay
	Lower Estuarine (E)	Peats and organic soft clays (discontinuous)
	Lower Fluvial Sand (F1)	predominantly loose sand (discontinuous)
	Lower Fluvial Clay (F2)	mainly firm clays (discontinuous)
Old Alluvium	Weathered (OAW)	discontinuous – Sands & Clays N < 30
	Slightly weathered (OA-SW2)	30 < N< 50
	Slightly weathered (OA-SW1)	50 < N< 100
	Cemented unweathered (OACZ)	N>100

Table 1: Soil Profile Description (MOM, 2005)

The soil profile (Figure 8 and Table 1) comprises deep layers of marine (MC), estuarine (E) and fluvial (F2) clays overlying much stronger layers of old alluvium (SW, CZ). The engineering properties to be used in the original design were specified in a Geotechnical Interpretative Memorandum (GIM). Please refer to Table 2 for more information on these parameters.

Following the collapse, a joint committee of experts reviewed the GIM Table of parameters and concluded that the parameters were generally reasonable with a couple notable exceptions:

1. Permeability properties of the Old Alluvium were difficult to estimate. In general, the clays and old alluvium layers are of low permeability.
2. Undrained shear strengths in the Lower Marine Clay (LMC) were potentially than the GIM recommendations (based on an interpretation of piezocone penetration data). Field monitoring of on-going settlements and pore pressures in the M3 are suggested that the LMC layer was under-consolidated, and this may explain why lower shear strengths can ocurr in this layer.
3. The GIM Table overestimated the undrained shear strength of the Lower Estuarine Clay due to extrapolation of properties from the Upper Estuarine Clay.

3.3 Plaxis Analyses

Plaxis is a general purpose geotechnical finite element program suitable for modeling a wide range of geotechnical processes. For the original design, a Plaxis model was generated to find the maximum design loads, moments and deflections for the diaphragm walls and cross-lot strut elements. The basic input parameters used in Plaxis to represent the various soil layers are summarized in Table 2.[1]

[1] Note that some of the input parameters used in the original analysis/design were incorrect. A new Plaxis model has been generated (see Chapter 4) with the corrected soil parameters.

Stratum	Material Type	Unit Weight kN/m^3	Perm m/day	Yref mRL	Eref MN/m^2	Einc $MN/m^2/m$	Cref kN/m^2	ϕ' Degrees	R inter
Fill	Drained	19	$8.6E10^{-2}$		10		0.1	30	0.67
Estuarine	Undrained	15	$8.6E10^{-5}$	92.9	6	0.92	0.1	18	0.67
M2(upper)	Undrained	16	$8.6E10^{-5}$	87.9	8	0.64	0.1	22	0.67
F2	Undrained	19	$8.6E10^{-5}$	92.9	8	0.8	0.1	24	0.67
M3(lower)	Undrained	16	$8.6E10^{-5}$	87.9	8	0.64	0.1	24	0.67
OA SW2	Drained	20	$4.3E10^{-2}$		70/72		5.0	32	0.67
OA SW1	Drained	20	$4.3E10^{-3}$		144/158		360/395	0	0.5
OA CZ	Drained	20	$4.3E10^{-3}$		200		500	0	0.5
JGP	Non por	16	0		131		300	0	0.33
OAClayN16	Undrained	20	$4.3E10^{-2}$		32		80	0	0.5
OASandN20	Drained	20	$4.3E10^{-2}$		40		0.1	32	0.67
OASandN26	Undrained	20	$4.3E10^{-2}$		52		130	0	0.5

Table 2: Summary of Plaxis Input Parameters in Original Design (MOM, 2005)

The most significant aspects of the original Plaxis analysis are as follows:

1. The Soil layers are represented as linearly elastic-perfectly plastic materials, with shear strength governed by the Mohr-Coulomb criterion with effective stress strength parameters (c' and φ').
2. Each of the low permeability clay layers is treated as undrained material, while old alluvium is assumed to be fully drained.
3. The JGP layers are assumed non-pourus with a cohesive component of shear strength, Su= 300kPa.
4. Pore pressures in the Old Alluvium were established by specifying a phreatic line , with reduced pressures below the base of the excavation.

More detailed background information on the use of Plaxis and the parameters included will be provided in Section 4 of this thesis.

3.4 Design of Structural Elements

The original design of the temporary wall and strutting system was carried out with the following assumptions: (using the British Standard Code of Practice for Earth Retaining Structures BS8002)

1. Effective stress strength parameters for characterizing the marine and estuarine clays at the excavation site.
2. Load factor of 1.2 for structural elements as per British Standard Code of Practice for Steel Elements (BS5950).
3. Surcharge load of 20 kPa, with actual surcharge not to exceed 10 kPa.
4. One strut failure analysis at selected locations.

For design purposes, the cut and cover tunnel was divided into 40 wall sections (approx. 6m each). The selection of wall type was based on an assessment of the soil profile, in particular the depth of the marine clays, and depth and width of the excavation.

3.4.1 Design of Diaphragm Wall in Type M3 Area

The diaphragm wall in Type M3 area had 10 levels of struts, and 2 levels of JGP slab. The upper JGP slab was located between the 9^{th} and 10^{th} level struts. The design required that the wall was embedded 3 meters in the Old Alluvium (SW2) layer. The soil profiles, strutting levels and JGP slab levels are presented in Figure 9. (Note that the spacing in the horizontal direction of the struts was 4m).

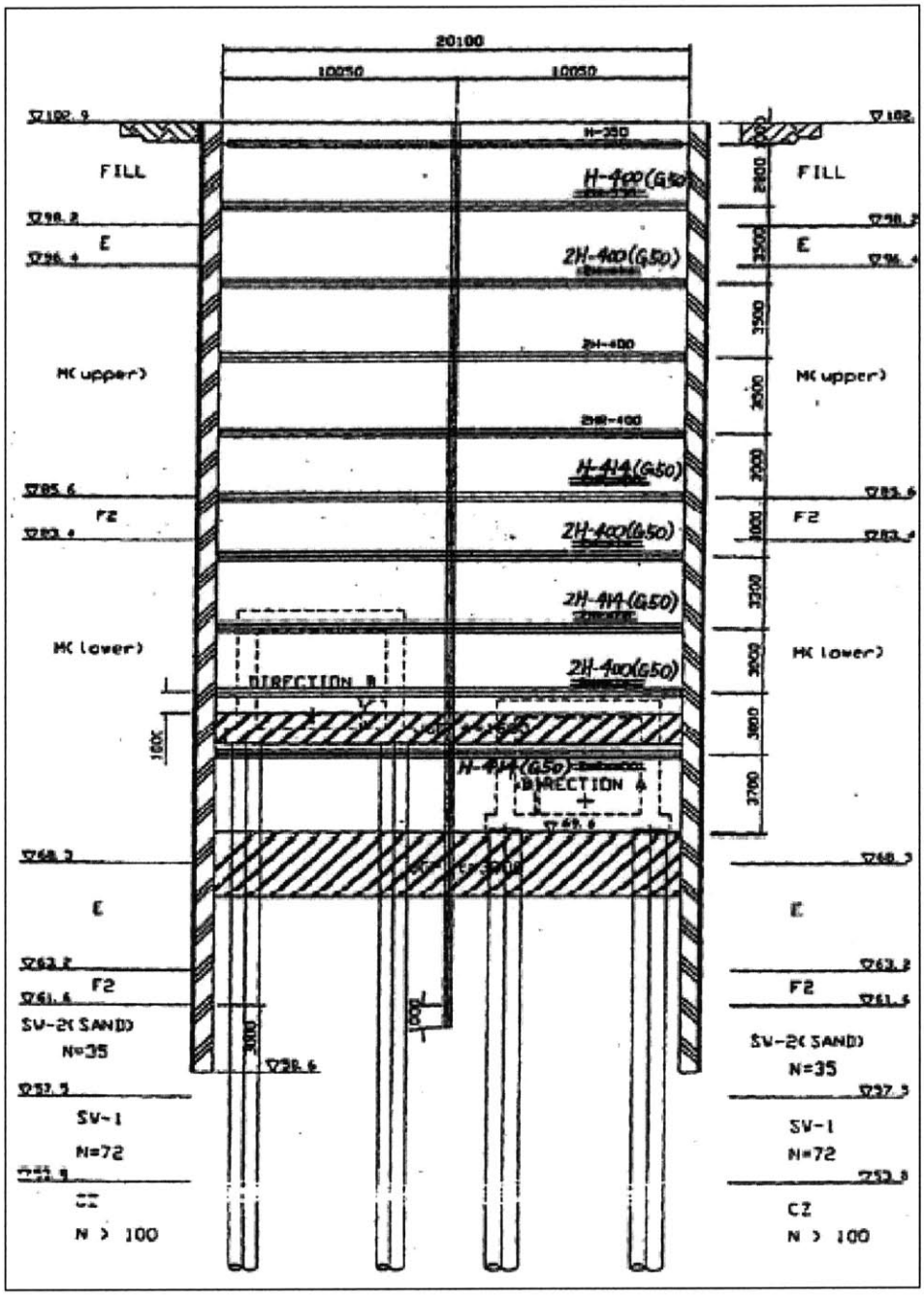

Figure 9: Cross-section for wall Type M3 (MOM, 2005)

Apparently, the incorporation of JGP slabs was done to help cut off soil seepage and reduce the need for further embedment of the diaphragm wall into the Old Alluvium (SW2). This was done in order to control the potential consolidation settlements outside the excavation.

The Plaxis results were used directly for the structural design of the diaphragm walls and strutting system. As mentioned earlier, the structural design adopted a 1.2 factor of safety provided that the "worst credible" soil parameters were used in the model. The load factor of 1.2 was applied to the bending moments and shear forces observed from the Plaxis output, and the ultimate design values were then used to determine the required steel reinforcement at various levels in the diaphragm wall panels. Checks for punching shear and wide beam shear were also performed in this design. The detailed calculations of the diaphragm walls can be seen in Appendix A.

3.4.2 Design of the Strutting System for Diaphragm Wall in Type M3 Area

The strutting system comprised steel H-sections (W-sections as per AISC) spanning between the diaphragm walls. Each strut was comprised of either a single or a pair of H-sections (Types shown in Figure 9 and Appendix B). The width of each diaphragm wall panel was 6m and the struts were spaced horizontally every 4m. The strutting system was arranged so that alternate panels were either supported at their mid-point by a strut or towards their edges by a strut at each edge. The majority of the struts were designed to bear directly against the wall panel, which had been reinforced accordingly. However, in certain occasions where splayed struts were required, a short waler beam was adopted in the design. The waler beams had to be discontinuous due to the curvature of the cut and cover tunnel.

The maximum strut load for each level of the struts was computed from the Plaxis analysis. Once the factor of safety (1.2) was applied and the ultimate design axial loads were obtained, the struts were checked to resist buckling. The detailed calculations of the strutting system can be found in Appendix B.

3.4.3 Design of Strut-Waler Connection

The waler beam design was comprised of steel beams that were of the same size as the connecting strut. A concrete packing was used to spread the load from the waler beams into the wall. Steel stiffeners were incorporated at the connections between struts and walers to prevent local buckling of the waler beam web. Please refer to Figure 10 for an illustrative view of the strut-waler connection.

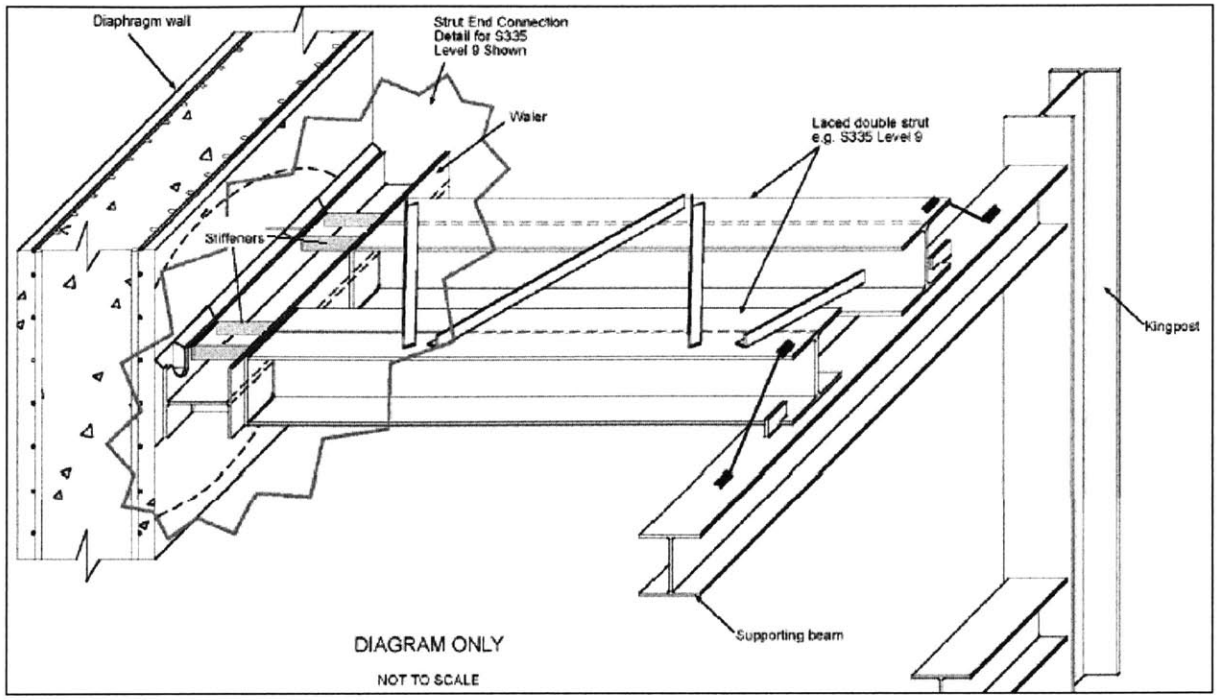

Figure 10: Strut-Waler Connection (Modified from MOM, 2005)

3.5 Construction Sequence

The construction sequence that was planned for the braced excavation system included:

1. Install diaphragm walls: After excavating a trench for the diaphragm walls and placing all the reinforcing steel for the wall panels, concrete was to be poured and cast on site to build the diaphragm walls around the perimeter of the excavation.
2. Drive kingposts: Once the diaphragm wall was in place, kingposts were to be driven at the specified locations (midpoint between the north and south walls and spaced horizontally every 4 meters)
3. Jet Grout Piling (JGP): Holes for interlocking Jet Grout Piles (JGP) were to be perforated at the specified locations of the design drawings in order to support the jet grout slabs shown in Figure 9. The thickness of the upper and lower slabs was 1.5m and 2.6m, respectively.
4. Install bored piles: JGP were to be bored once the holes were perforated.
5. Excavate up to 0.5m lower than the 1st level struts: Excavation was to be carried out down to an elevation of 0.5m below the first level of struts. Please refer to Figure 9 for more information on strut level elevations.

6. Install pre-loaded struts: The first level of pre-loaded struts was to be placed and framed to the diaphragm walls or waler beams (depending on the location) at the specific points determined in the design. (First level struts were spaced horizontally every 8m).
7. Excavate up to 0.5m lower than the next level struts: Following the installation of the struts, excavation was to be resumed at an elevation of 0.5m below the second level of struts.
8. Install pre-loaded struts: The second level pre-loaded struts were then to be installed and spaced every 4m in the horizontal direction of the wall.
9. Repeat steps 7 to 8 until the lowest struts (10^{th} level) were installed and pre-loaded
10. Excavate to formation level: Once the 10^{th} level struts were installed, excavation to formation level was to be performed and 75mm thick lean concrete was to be cast without delay.

4. The Collapse

At about 3:30pm on April 20, 2004, a 30m deep excavation adjacent to Nicoll Highway in Singapore collapsed resulting in four casualties and a delay of part of the US$4.14 billion CCL subway project. According to the Committee of Inquiry (MOM, 2005) that was set up to investigate the failure, the main causes of the collapse included two critical design errors in the temporary retaining wall system. These were:

1. The under-design of the diaphragm wall using Method A[2]. The use of Method A in the original design to model the undrained behavior of soft marine clays was incorrect. The method over-predicted the undrained shear strength. In other words, it underestimated the bending moments and deflections of the diaphragm wall. Hence, this resulted in an under-designed diaphragm wall. Method B should have been used in this circumstance. The bending moments and deflections in the original design were about 50% of the actual bending moments and deflections observed by the diaphragm wall. This is equivalent to a factor of 2 in the original design of the diaphragm wall in the Type M3 area.

2. The under-design of the strut-waler connection in two ways:
   a) The original estimation of load on the strut-waler connection for double struts assumed that the splays would absorb one third of the load in the struts. Where splays were omitted, the design load that resulted in the strut-waler connection was only about 70% of the load in the strut, when the full 100% should have been used.
   b) The change in the design of the waler plate stiffeners with C-sections (Figure 11) relied on a stiff bearing length (b1) of 400mm instead of approximately 65mm in accordance with BS5950, and on an effective length of 70% of the net web depth, where a number close to 1.2 for unrestrained conditions would have been more appropriate. As a result, the axial design capacity of the stiffeners was only about 70% of the assumed design load for the connection. Further explanation of this will be provided later in this section.

[2] Method A refers to the use of effective stress strength parameters to represent the undrained shear strength of low permeability clay. Further explanation will be given in later sections

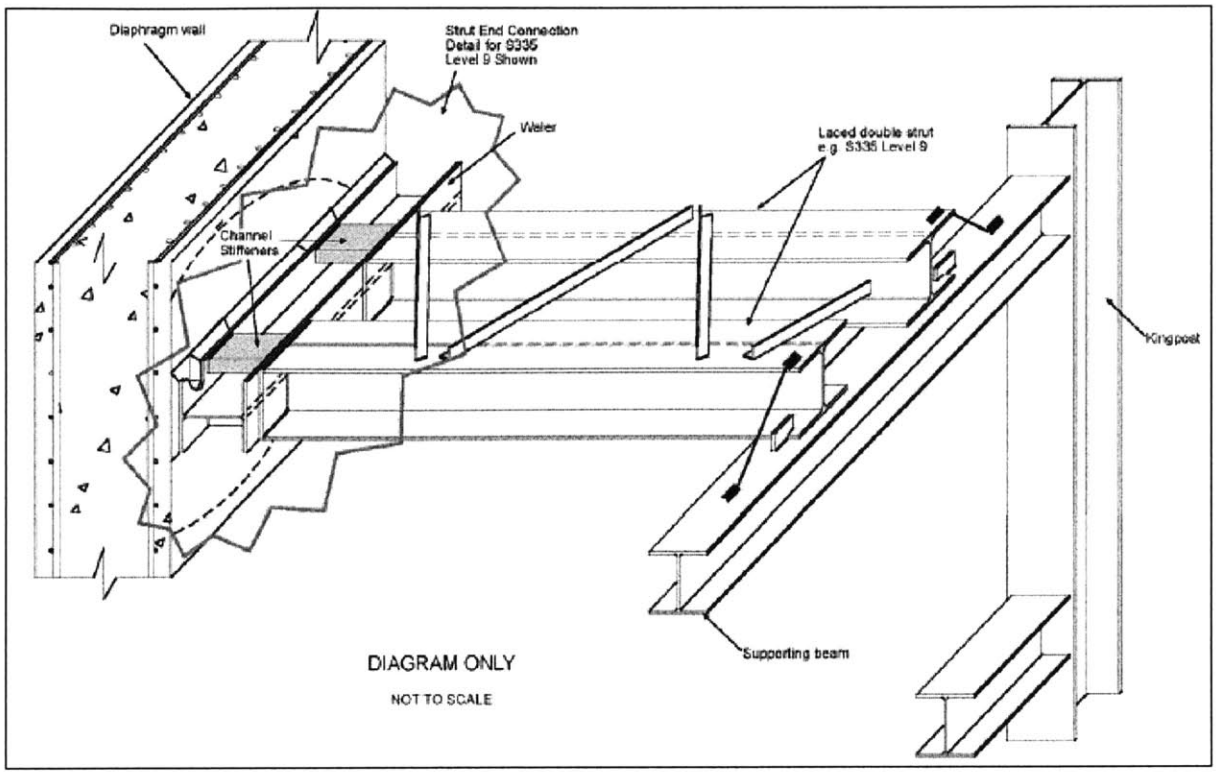

Figure 11: Strut-Waler Connection Channel Stiffeners (MOM, 2005)

The under-design of the waler connection caused the failure of the 9th level strut-waler connections at the Type M3 area during the excavation to the 10th level. This was the initiating failure of the collapse. The failure of the 9th level waler connection caused the transfer of loads to the 8th level struts, leading to the failure of the 8th level strutting system and the subsequent collapse of the Type M3 area. The collapse then propagated westward to the Type M2 area.

Other errors such as inadequate welding of the members could have also contributed to the collapse of the excavation system, but these factors were not as critical as the two specified previously. The failure of the 9th level strut-waler system together with the inability of the temporary retaining wall system to resist the redistributed loads as the 9th level strutting failed led to a catastrophic collapse of the excavation system (Figure 12).

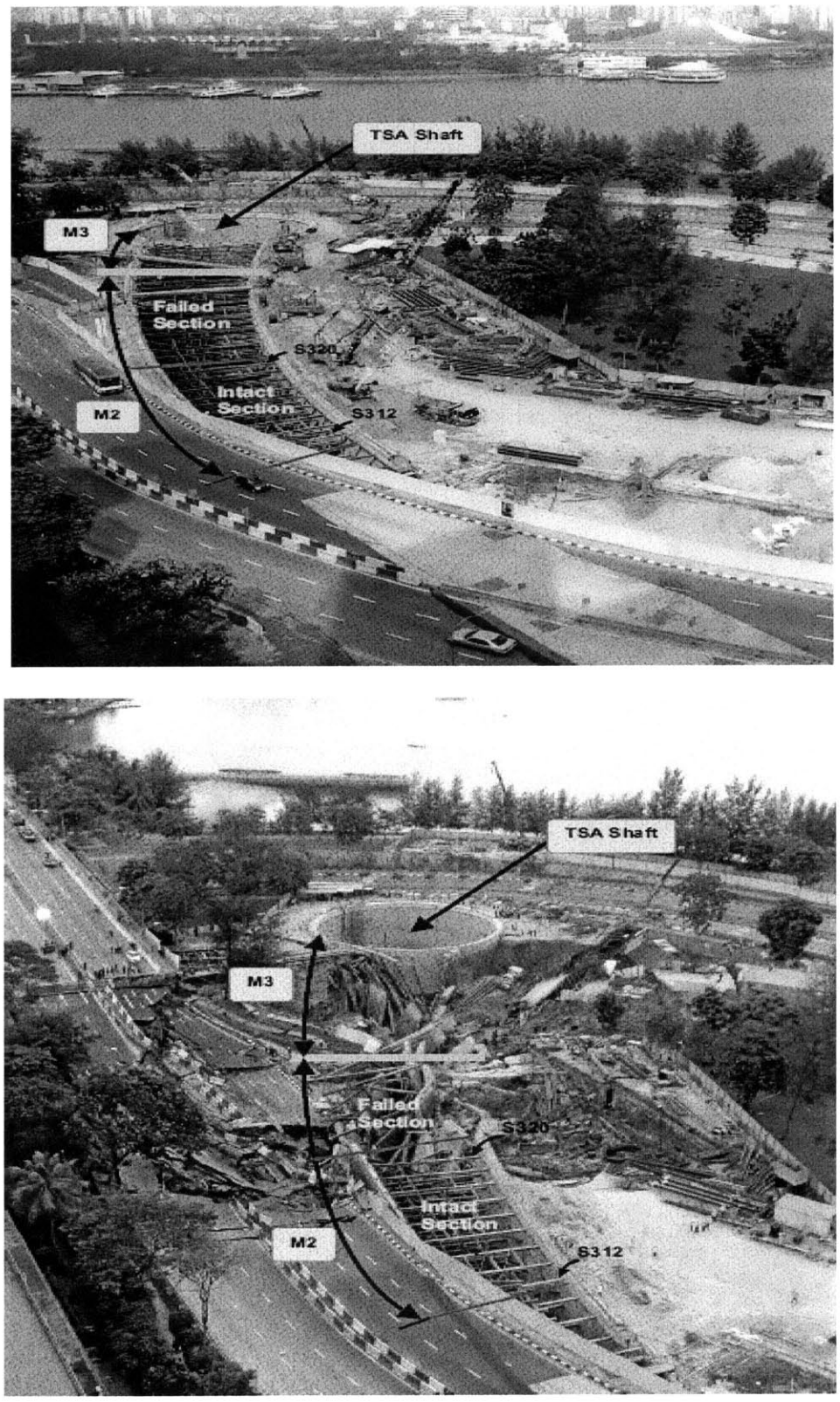

Figure 12: Site Before and After the Collapse (MOM, 2005)

4.1 The Under-design of the Diaphragm Wall Using Method A

In order to appreciate the impact of Method A on the temporary retaining wall system, it is necessary to provide background information with respect to the design of the temporary retaining wall system and sufficient detail concerning the Plaxis finite element program.

A user with a sound understanding of the theoretical basis of the Mohr-Coulomb model and soft soil behavior would realize that Method A could not model the stress-strain response of soft clays correctly. For soft, normally to lightly over-consolidated clays, the use of effective stress parameters in a Mohr Coulomb model with undrained material setting will inevitably lead to the over-prediction of undrained shear strength. The problem inherent in Method A was therefore a fundamental error in the original design. (MOM, 2005, Ch. 5)

4.1.1 Background and Errors in the Input Data of the Plaxis Finite Element (FE) Program

Plaxis is designed to perform numerical analyses of deformation and stability of geotechnical problems. It contains a number of features to handle aspects of geotechnical engineering that are often specific to the given site. In particular, the consideration of soil as a multi-phase material leads to the provision of special procedures for dealing with the modeling of the *in-situ* (on site) stress state, simulation of fill placement and excavation, and the generation and modification of pore water pressures in the soil. (MOM, 2005, Ch. 5)

Material Types (Drained, Undrained, and Non-porous)

Plaxis allows the user to select different material types (Drained, Undrained, and Non-porous). In geotechnical engineering, the response of a saturated soil to changes in loading condition is broadly divided into undrained and drained behavior. Plaxis also includes a third type of material referred to as *Non-porous*. When a saturated soil of low permeability is loaded quickly such that water has no time to escape from the pore spaces, the pressure in the pore fluid will change. Since the amounts of solids and water do not change during the loading process, the volume change during loading is nearly zero. This type of soil is considered *undrained*. The rate of loading for which the soil behavior may be considered *drained* or *undrained* is a function of its permeability and drainage condition. When a saturated soil has high permeability, or when it

is loaded sufficiently slowly so that water can flow and escape from the voids without generating any additional pore pressures, its condition is then considered *drained*. The flow of water in and out of the pore spaces will therefore induce volume change in the soil mass. The *Non-porous* material type is considered impermeable and does not include any assessment of pore water pressure. (MOM, 2005, Ch. 5)

Material models

Plaxis provides several material models of varying complexities to model the behavior of soils. Each material model provides a mathematical representation of the stress-strain and strength characteristics of the soil. The choice of soil model controls the way in which pore water pressures are calculated during the undrained loading stages.

The Mohr-Coulomb model was used for all the soil strata and the JGP in the original Plaxis model. This model assumes the material exhibits isotropic linear elasticity until it reaches yield. Changes in the shear stresses applied to a Mohr-Coulomb model generate shear strains but no volumetric strain. Changes in the mean effective stress in the Mohr-Coulomb model generate volumetric strains but no shear strain. This type of model does not present any volumetric strain due to shear. As a consequence, the soil must follow a constant stress (p') path in response to undrained loading. A failure of the soil to resist the loading conditions will occur at a point where the initial effective mean stress (p') at the start of the loading sequence meets the Mohr-Coulomb failure line in the p-q space (O-B-A, Fig.11). (MOM, 2005, Ch. 5)

Most real soils undergo some volumetric change as a result of shearing under drained conditions. In particular, it is well established that soft, normally consolidated or lightly over-consolidated clays tend to contract as a result of drained shearing. In undrained loading in which the soil matrix is prevented from contracting, this contractive tendency will be manifested as positive pore water pressure within the soft clay. As a result, the soft clay follows an effective stress path that curves back from the constant stress line (p'), thus reducing the mean effective stress during the loading stage, as illustrated by path O-D in Figure 13. (MOM, 2005, Ch. 5)

Due to the contractive nature of the soft clay, the undrained strength (D, Fig.11) is less than the drained strength. Since the Mohr-Coulomb model does not model this contractive effect, it cannot reproduce the stress path followed by the soft clay as it is sheared. The Mohr-Coulomb model using effective stress strength parameters therefore over-estimates the strength of soft normally consolidated clay in undrained condition. (MOM, 2005, Ch. 5)

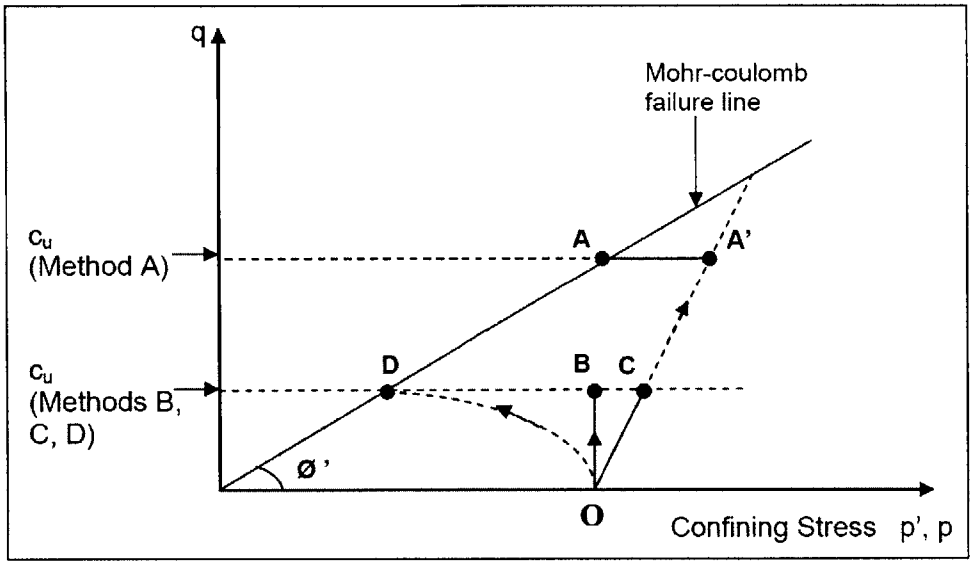

Figure 13: Mohr-Coulomb Failure Model (MOM, 2005)

(Undrained shear strengths derived from Methods A, B, C and D used in the original design)

The Mohr-Coulomb model allows the user to input either effective stress parameters (c' and φ') or the undrained strength parameters ($c'=c_u$, $\varphi'=0$). Although this approach would give the correct undrained strength, it cannot correctly model the stress path followed by the soft clay. (MOM, 2005, Ch. 5)

In the original design, the use of a Mohr Coulomb soil model with effective stress strength parameters in combination with an undrained material type has been referred to as Method A. Method B refers to the use of Mohr-Coulomb soil model with undrained strength parameters in combination with undrained material type. The latter method prevents the Mohr-Coulomb model from over-estimating the strength of soft clay in undrained condition (as shown in Fig.11).

The pore water pressure generated by the Mohr-Coulomb model will not be representative of those generated *in-situ* under an undrained loading condition. This is true regardless of whether the effective stress parameters (Method A) or the undrained parameters (Method B) are used. The parameters used for the various methods are tabulated in Table 3.

Undrained Behaviour					
Method	**Plaxis Material setting**	**Material Model**	**Parameters**		**Computed stresses**
			Strength	**Stiffness**	
A	Undrained	Mohr-Coulomb	c', ϕ' (effective)	E',ν' (effective)	Effective stress and pore pressure
B	Undrained	Mohr-Coulomb	c_u, ϕ_u (total)	E', ν' (effective)	Effective stress and pore pressure
C	Non-porous	Mohr-Coulomb	c_u, ϕ_u (total)	E_u, ν_u=0.495 (total)	Total stress
D	As in Method A, for other soil models				

Table 3: Plaxis Parameters under Different Design Methods (MOM, 2005)

Pore Water Pressure Distribution

There are two calculation types available in Plaxis, referred to as Plastic and Consolidation analyses. The Plastic calculation type is the non-linear computation carried out for loading stage, such as surcharge placement or an excavation with changing applied loads. Plastic calculation steps do not consider time-dependent phenomena such as consolidation or pore pressure dissipation. The consolidation calculation type refers to a stage involving consolidation or seepage in which excess pore water pressure will change with time. For the consolidation type of calculation, the Plaxis program computes the groundwater flow and the volumetric consolidation or swelling of the ground caused by changes in the mean effective stress. (MOM, 2005, Ch. 5)

The Plaxis analyses used in the original design did not make use of the seepage and consolidation capabilities within Plaxis. Only Plastic analyses were used in modeling all the construction stages, with no seepage or consolidation.

Nevertheless, instead of determining the groundwater pressure distribution by seepage and consolidation analyses, it is possible to input the groundwater pressure profile directly into Plaxis. An approximate and simple method is to assume that the groundwater is hydrostatic below a pre-defined water table.

This was the method adopted in the original analysis. It was assumed that the groundwater table outside the excavation was at the ground surface. Inside the excavation, the groundwater table was assumed to coincide with the base of the excavation and was changed concurrently with the excavation stages. (MOM, 2005, Ch. 5)

Specifying the water profile in this manner was a gross oversimplification of the real groundwater pressure system resulting from the excavation, and had the following shortcomings:

1. At and directly below the toe of the diaphragm wall there is a step change in the water pressure profile. On the excavation side, the water pressure is hydrostatic (changes linearly with depth) from the excavation surface. However, on the retained side of the wall the water pressure is hydrostatic from the *original* ground water table. This step change in pressure can never occur in the real situation.
2. The method cannot be used to study the effect of increasing pore pressure beneath the excavation as a result of seepage and consolidation processes.

4.1.2 The Impact of Method A and Method B on the Diaphragm Wall Design

The model used in the original design adopted Method A for the Estuarine clay, Marine clays (upper and lower) and Fluvial clays. As mentioned previously, Method A used the effective parameters (c' and φ') and Method B used the undrained strength parameters (c'=cu, $\varphi'=0$). A revised model was generated adopting Method B for *all* the soils specified above, while maintaining a *ceteris paribus* state in the model (all else being equal).

Figure 14 presents a comparison of the predicted displacements for wall Type M3 under each method. The predicted displacements using Method B are more than 100% greater than the Method A prediction.

Figure 15 shows a comparison of the predicted bending moment profiles for wall Type M3 under each method. The figure also includes the as-built moment capacity. The unfactored bending moments predicted using Method B exceeded the as-built moment capacity of the wall by more than 100% at several locations.

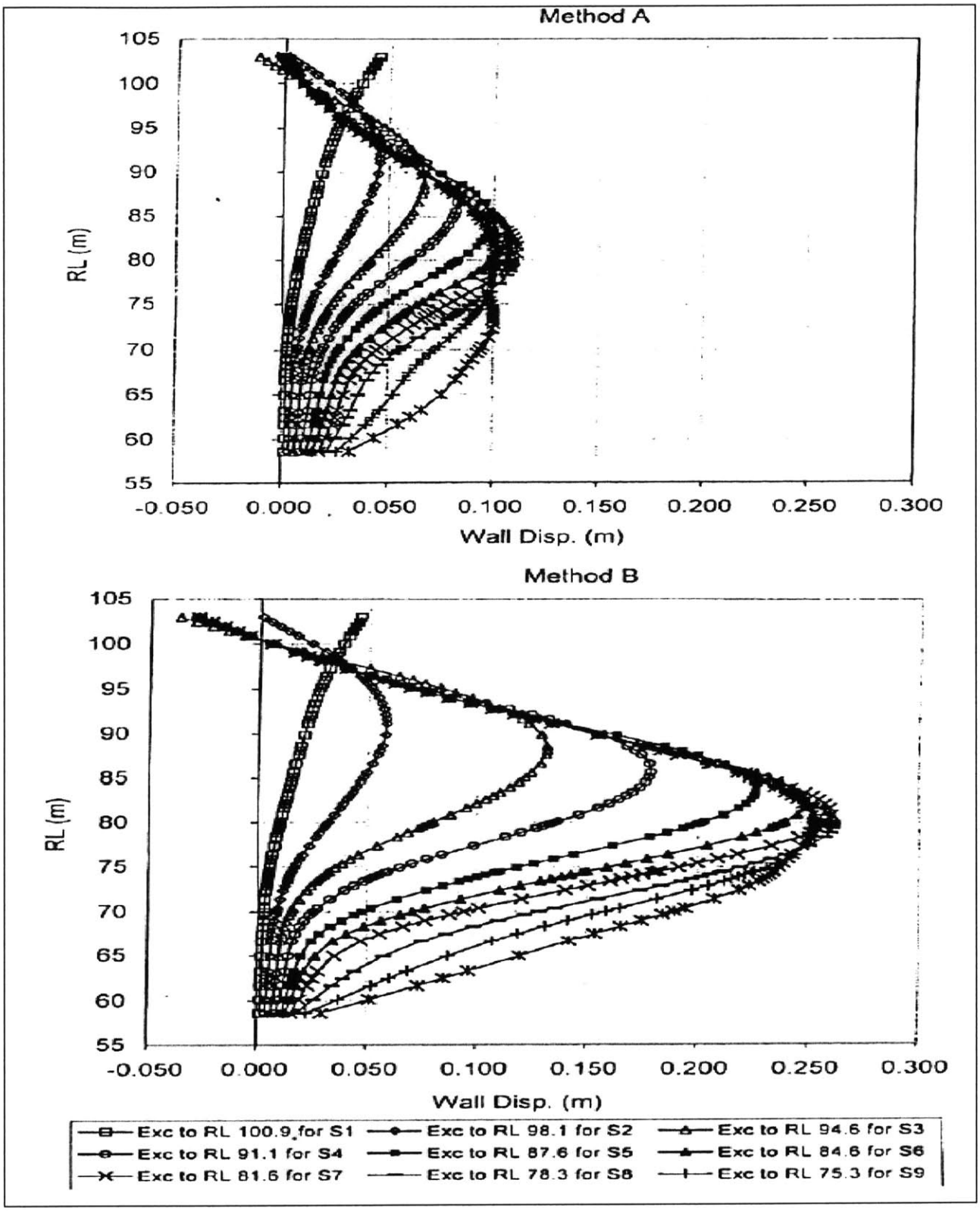

Figure 14: Diaphragm Wall Deflections under Methods A and B (MOM, 2005)

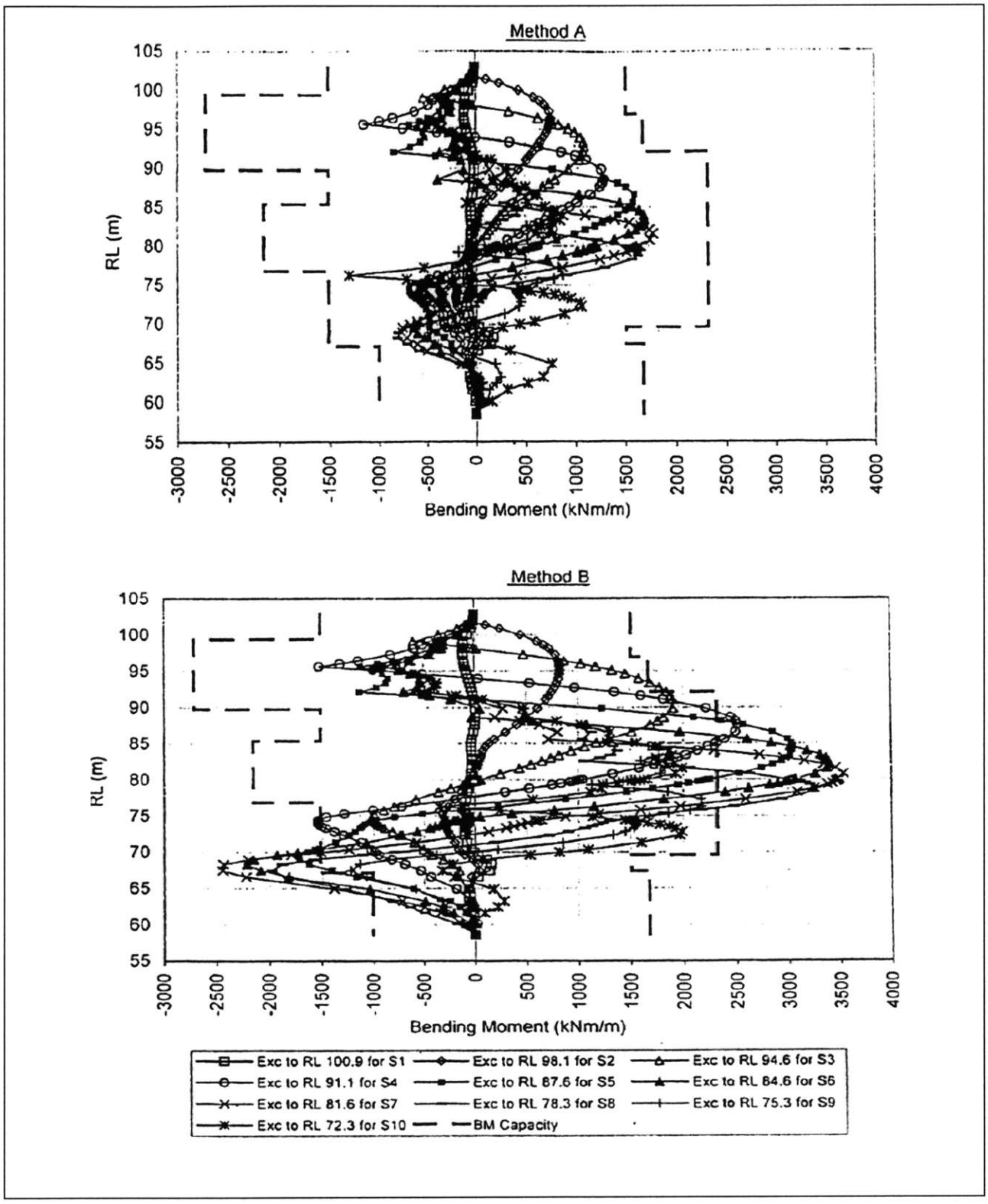

Figure 15: Diaphragm Wall Bending Moments under Methods A and B (MOM, 2005)

It is clear from the results that Method A under-predicted both, bending moments and displacements of the diaphragm wall. The retaining wall system designed using the results obtained from the Method A analysis was therefore severely under-designed. This led to the excess of the wall moment capacity and the formation of plastic hinges as the excavation reached deeper levels. For example, Figure 16 shows the wall deflections measured by two inclinometers (I-104, South and I-65, North) at type M3, for excavation immediately prior to failure on April 17.

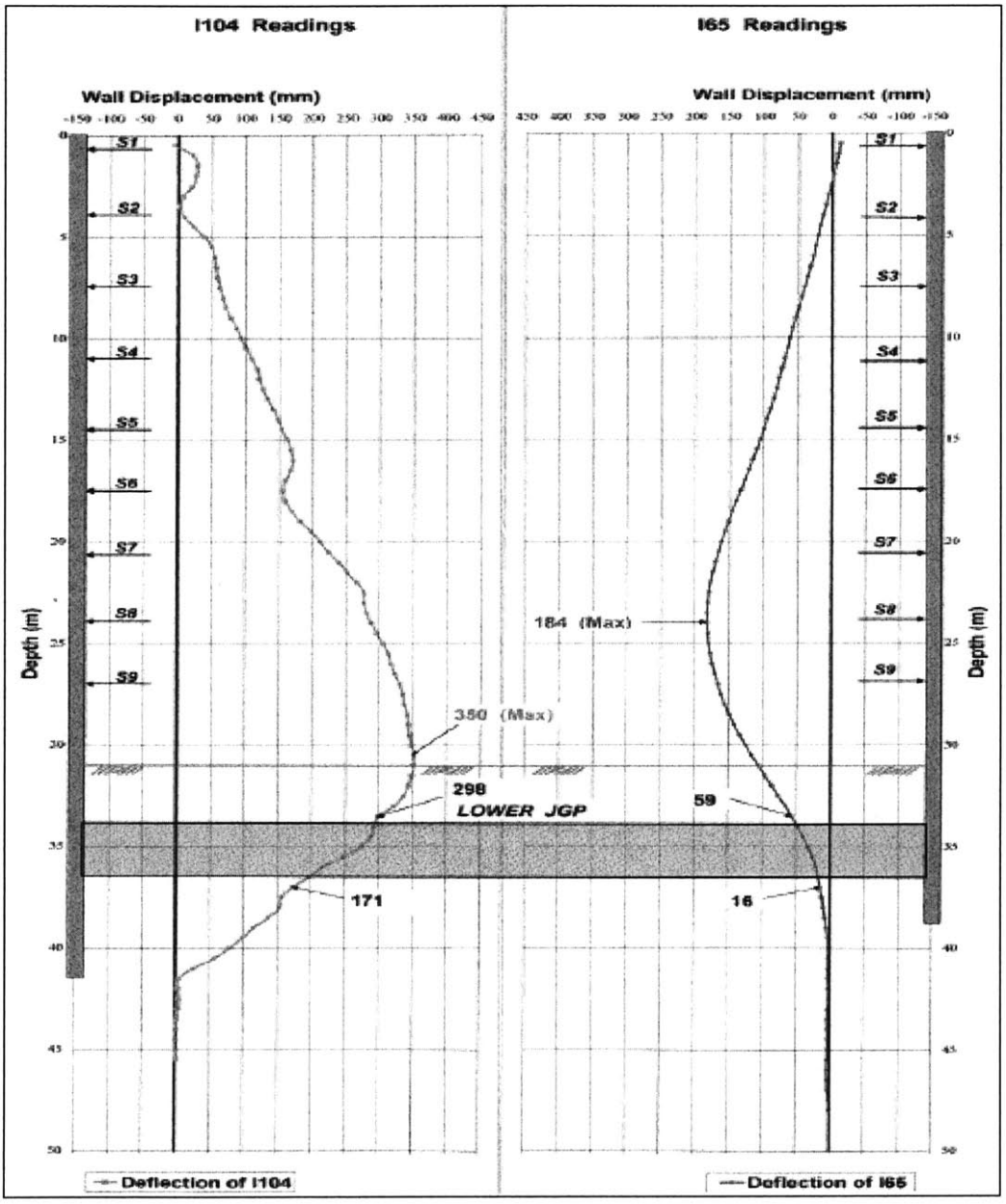

Figure 16: Inclinometer Readings I-104 & I-65 (MOM, 2005)

The use of Method B in the analysis resulted in a diaphragm wall design with thicker wall sections and possibly deeper penetration into the competent Old Alluvium.

4.2 The Impact of Method A and Method B on the Strutting System Design

The maximum predicted strut load at each level during the excavation sequence using Method B is given in Table 4 and is compared to the unfactored design of the strutting system.

Strut Row	Predicted Strut Load Using Method B (kN/m)	Design Strut Load (unfactored) Using Method A (kN/m)	Ratio Method B to Design Strut Load
1	379	568	67%
2	991	1018	97%
3	1615	1816	89%
4	1606	1635	98%
5	1446	1458	99%
6	1418	1322	107%
7	1581	2130	74%
8	1578	2632	60%
9	2383	2173	110%

Table 4: Strut Loads at Type M3 Area under Design Methods A and B (MOM, 2005)

The strut loads predicted by Method B and the design (unfactored) strut loads using Method A fall within a range of 60% to 110% of the original design value. For level 9, Method A resulted in the strut design being under-estimated by about 10% in comparison to Method B. However, the strut load for level 9 used in the revised design that is presented in Section 5 is less than that used under Method A (approximately 93% of 2173 kN or 2020 kN). Even though the revised design was performed using Method B, the variation of the loads in the revised design from the loads predicted by Method B in Table 4 are due to an increment in the thickness of the

diaphragm wall used in the revised design. Further explanation on this will be provided in Section 5 of this thesis.

4.3 Under-design of Strut-Waler Connection

In the original design of the strut-waler connection, the check for local buckling of the waler web used a wrong value of 400mm for the stiff bearing length. The correct value in a strict interpretation of the code BS5950 would be 65mm. Stiff bearing length has a direct correlation with the capacity of the waler system. A longer stiff bearing length produced a buckling resistance of the waler web in the design calculations. In spite of the error, it was found that the buckling resistance Pw was still less than the strut load bearing on the waler Pbr.

For H-400, which was used at the 9th level strutting system of the Type M3 area, Pbr was 3543 kN, while Pw was 2218 kN. This meant that the web could not, on its own, be able to withstand the forces acting on it and therefore stiffeners were required in order to increase the capacity of the connection against buckling. Please refer to Appendix C for details on these calculations.

The design error in the stiff bearing length, although not in accordance with BS5950, did not contribute materially to the capacity of the original stiffener design (using plate stiffeners) because the wrong waler web buckling capacity (Pw) was not used in this calculation set. The capacity of the H-400 waler section stiffened with a plate on each side of the web was calculated correctly as 2424 kN in accordance with BS5950.

The stiffener plates were crucial components of the strut-waler connection. The ability of the entire strut/waler connection to bear the forces acting upon it was dependent on the strength of the stiffened section. The integrity of the entire strutting system could be affected by the lack of adequate capacity in the strut-waler connection to withstand the load. It was therefore critical that the design of the stiffeners (and any changes made to it) was carefully reviewed to ensure its adequacy and strength.

4.3.1 Incorporation of C-channel Stiffeners in Waler Beam Connections

In February 2004, several instances of buckling of the stiffener plates and waler webs were reported at the Nicoll Highway Station (Figure 17).

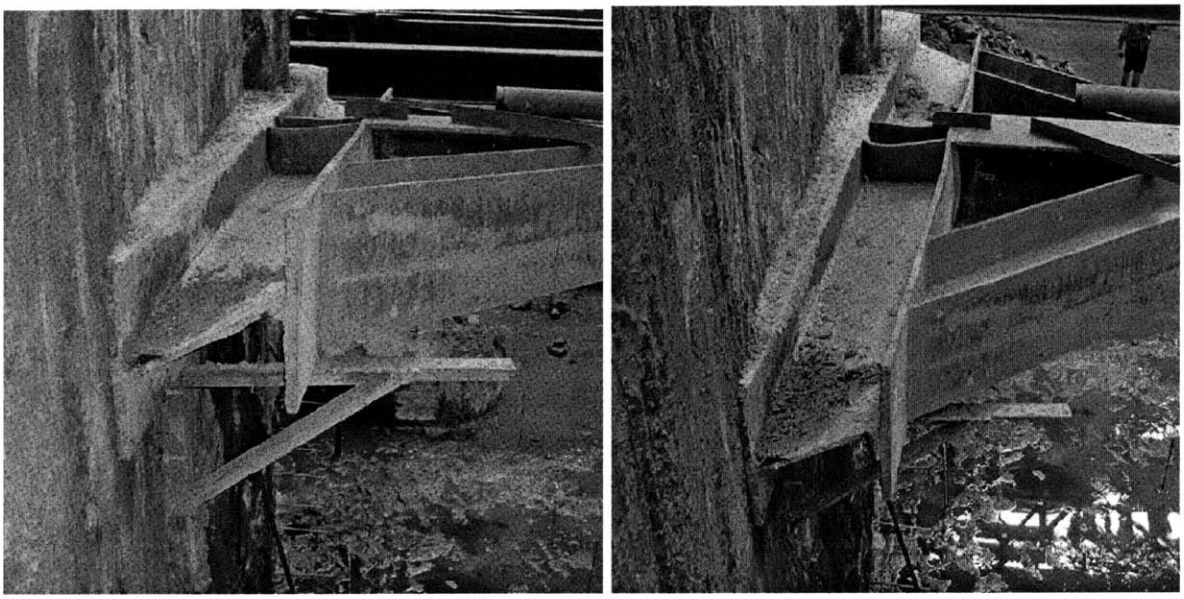

Figure 17: Stiffener Plate and Waler Beam Web Buckling (MOM, 2005)

This condition led the contractor to replace the double stiffener plates with C-channel sections. The replacement of double stiffener plates with C-channels provided only minor improvement to the design in terms of axial load bearing capacity for the waler connections, but this came at the expense of ductility. The change worsened the design and made it more susceptible to the brittle "sway" failure mode. This is proved *a posteriori* in the results of finite element analyses and physical laboratory tests that were performed by experts after the collapse occurred.

Finite element calculations showed that in the elastic range, the C-channels attracted about 70% of the axial strut load. This caused the yielding of the C-channels before the web reached its full capacity. Once the C-channel had yielded completely, a fundamental change in the behavior of the connection occurred: the resistance of the waler flanges to relative displacement (i.e. lateral sway) was reduced. As the axial compression continued, local crushing of the web occurred. At this point, there was little resistance to rotation and lateral displacement

on the outer (towards the excavation, away from the wall) waler flange. The results post-collapse demonstrated clearly that the connection was susceptible to sway failure under direct compression.

Once the axial force reached the yield capacity of the C-channel connection, the connection displayed a very brittle response, resulting in a rapid loss of capacity upon continued compression. Conversely, the plate stiffeners connection was significantly more ductile. Please refer to Figure 18 for a graphical visualization of this fact.

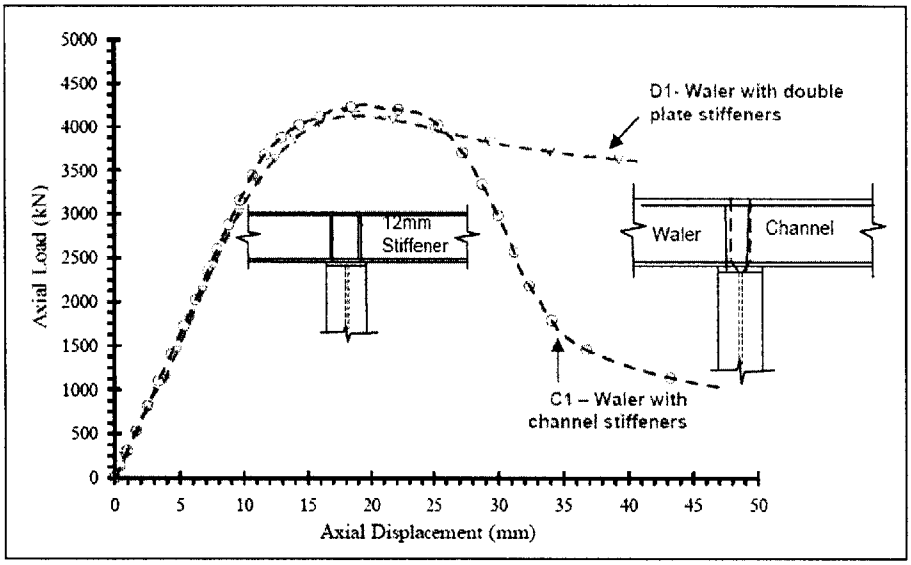

Figure 18: Load-Displacement Curves of the C-channel and Plate Stiffener Connections (MOM, 2005)

This graph proves that the failure load / peak capacity of waler with C-channel stiffeners is about equal to that with double plate stiffeners. However, the C-channel stiffeners accentuated the problem associated with the under-design of the waler connections because they induced the sway mode of failure into the strutting system. When the C-channel was compressed beyond the peak capacity, there was a rapid and sudden release of load, resulting in a large reduction of the capacity of the C-channel connection beyond yield, thereby causing a brittle failure.

4.3.2 Omission of Splays in Strut-Waler Connections

The strut to waler connection detail adopted one of three possible arrangements depending on whether it was a single or double strut and if splays were to be used or not. The estimation of load on the strut-waler connection for double struts assumed that the splays would absorb one third of the load in the struts (Figure 19).

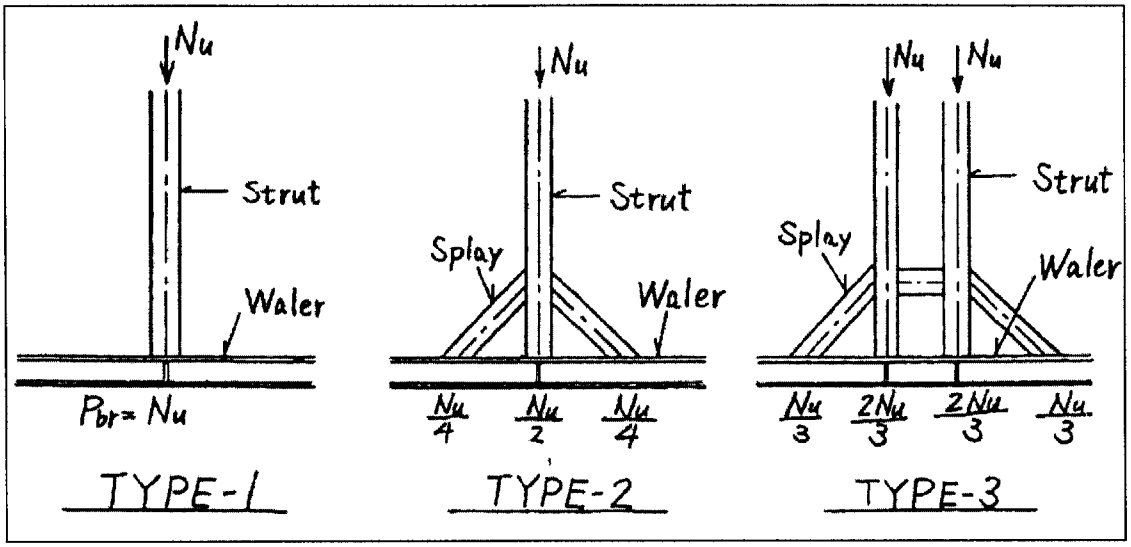

Figure 19: Types of Strut-Waler Connections (MOM, 2005)

The original design of the double struts at the 9th level of the excavation in the Type M3 area calculated a maximum strut force (including all factors of safety) of 5314 kN per H-section. On the assumption that splays would be included, the design load at the strut-waler connection was reduced to 3543 kN. All of the strut-waler connections on the 9th level of Type M3 were designed to withstand a load of 3543 kN. During construction, however, there were a number of struts on the 9th level that were not provided with splays. The strut-waler connection therefore had to sustain the entire strut load of 5314 kN. This was far in excess of the 3543 kN for which they had been designed. Consequently, the connection as designed did not have the capacity to cope with the existing loads. Please refer to Appendix C for further details on these calculations.

For the strut-waler connections without splays, the combined effects of the errors in the stiffeners design and the omission of splays resulted in the design capacity of the connections being only about one-half of the required design strength.

5. A Revised Design for the Type M3 Excavation Area

This chapter proposes a revised design for the Type M3 excavation support system. This revised design is based on Allowable Stress principles for the revised design of the diaphragm wall, strutting system, and strut-waler connection. The factor of safety was therefore applied to the member capacities – as opposed to the loads exerted on the members (i.e. bending moments and axial loads).

5.1 Revised Plaxis Model

A revised Plaxis analysis of soil-structure interaction has been carried out for the Type M3 section using input parameters provided by Whittle. (Pers. Comm.)[3]. The main features of this revised analysis are as follows:

1. The undrained shear strength profile of the Estuarine, Marine and Fluvial clays has been supplied directly according to Method B ($c'=c_u$, $\varphi'=0$). The revised model parameters are listed in Table 5.
2. The Old Alluvium is also assumed to behave in undrained shearing.
3. The thickness of the lower JGP is revised to 2.6m to reflect the as-built conditions at Type M3.
4. The revised model assumes no reduction interface shear strength (i.e. R=1, refer to Table 2) between the cast *in situ* diaphragm wall and the adjacent soils.

[3] Referred to in expert report by Whittle, Andrew as Method B-var 7.

Layer	RL (m)	σ'_{v0} (kPa)	γ_t (kN/m^3)	k (m/day)	s_u (kPa) [c']	Friction angle, ϕ' ()	Shear Modulus, G (MPa)	ν'	K_0	Piezo-metric Head, H(m)
Fill	102.9 98.2	43	19.0	0.086	[0]	30.0	4.0	0.25	0.5	100.5
Upper MC	98.2 85.6	58 120	16.0	8.6 x 10^{-5}	20 25	0	3.0	0.25	0.7	100.5 103.0
F2 Clay	85.6 83.4	120 132	19.0	8.6 x10^{-5}	88	0	11.7	0.25	0.7	103.0
Lower MC	83.4 75.0 63.2	132 189 293	16.8	8.6 x10^{-5}	31 47	0	5.2	0.25	0.7	103.0 105.0 103.0
F2 Clay	63.2 61.6	293 309	20.0	8.6 x 10^{-5}	88	0	11.7	0.25	0.7	103.0
OA – weathered	61.6 53.9	309 386	20.0	8.6 x 10^{-4}	100 500	0	40.0	0.25	1.0	103.0
OA - competent	<53.9	386		8.6 x 10^{-5}	500	0	67.0	0.25	1.0	103.0
JGP	---		16.0	8.6 x 10^{-5}	300	0	108.0	0.15	--	--

Table 5: Summary of Soil Parameters used in Revised Plaxis Model

The output file of this analysis can be seen in Appendix D.

5.2 Design of the Diaphragm Wall

The bending stress was the greatest concern in the design of the diaphragm wall. Figure 21 summarizes the envelope of bending moments for the complete excavation sequence. The maximum moment, Mmax (+) = 6.21MN-m/m occurs at Elevation 71.6m, while much smaller bending moments occur at the back of the wall, Mmax (-) = 2.22MN-m/m at Elevation 68.3m.

As per AASHTO Standard Specifications for Highway Bridges (14^{th} Edition), the required area of steel needed to resist these forces could not be designed for a 0.8m thick diaphragm wall. Hence, the thickness of the wall must be increased in order to accommodate the number of rebars required in the design. However, increasing the wall size (and bending stiffness) generates even higher bending moments in the wall. An iteration process was done to obtain the optimal wall thickness and rebar area required. The final thickness of the wall was 1.2m, and the required area of steel per meter of wall was $42757mm^2/m$ on the near-end and $11600m^2/m$ on the far-end of the wall to resist positive and negative bending moments, respectively. The area of steel provided in the revised design was approx. 7.5 times higher for resistance of positive bending moments and 2 times higher for resistance of negative bending moments than the ones used in the original design. The maximum axial forces observed by the wall were also included in the analysis and slightly decreased the design bending moments of the wall. Please refer to Appendix E for further information on these calculations.

The total amount of rebar should be placed in the following manner to effectively resist the bending moments:
For the entire depth of the wall, # 14 bars should be spaced every 102mm on the front face of the wall to resist positive bending moments. On the rear face of the wall, # 9 bars should be spaced every 102mm to resist negative bending moments for the first 19m and the last 21.5m of wall depth. Please refer to Figure 20 for a sketch of the wall design with location of the rebars.

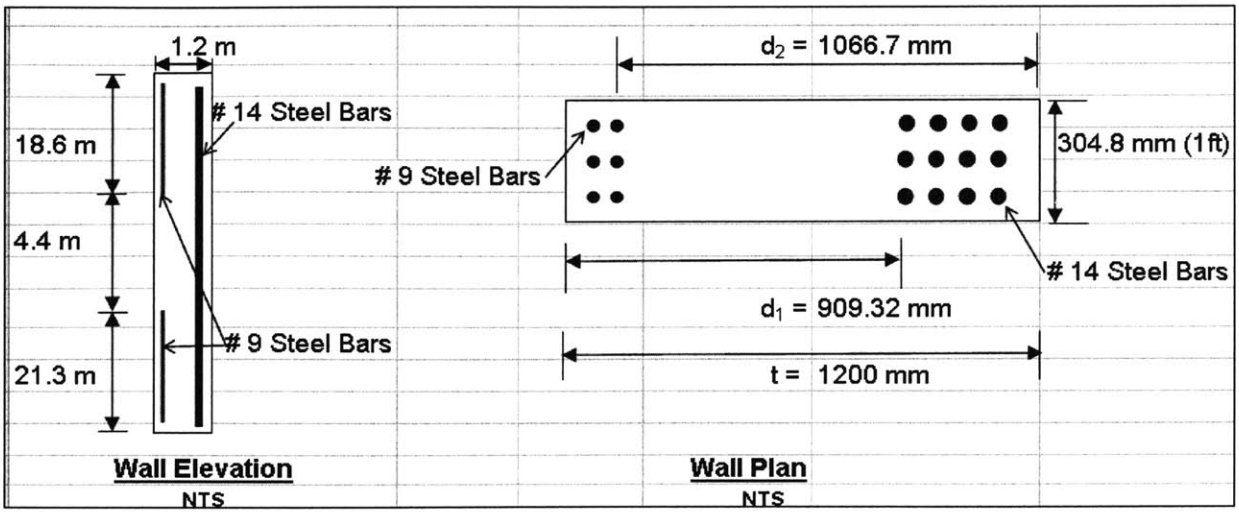

Figure 20: Sketch of Proposed Reinforcement for Diaphragm Wall (Plan and Elevation)

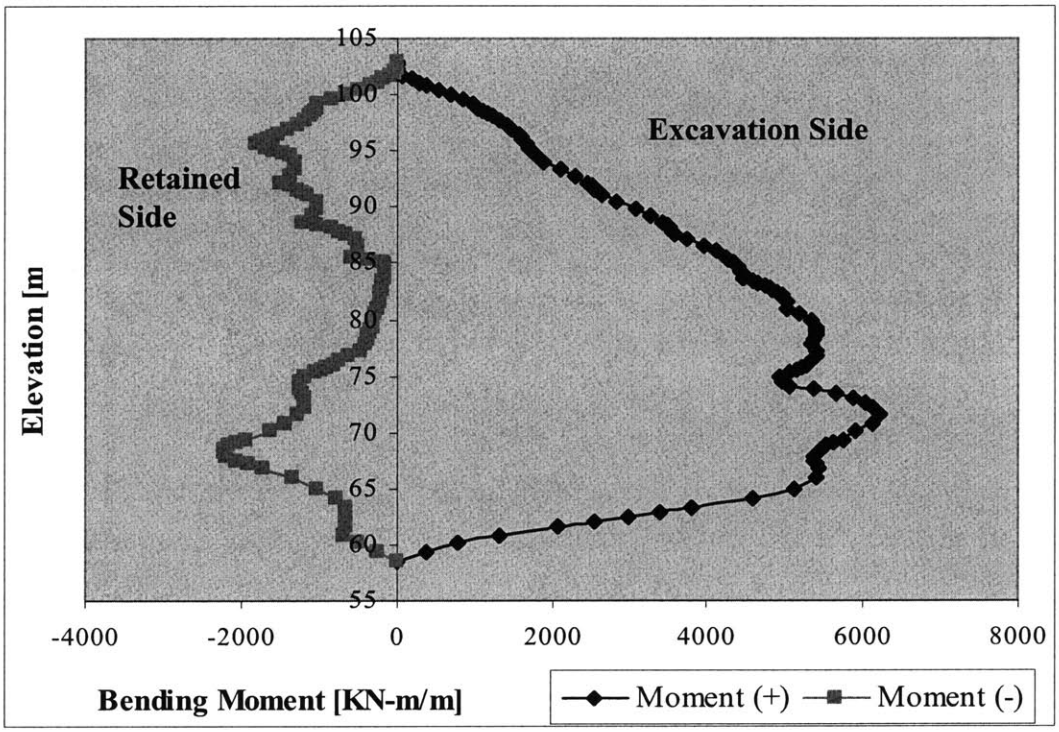

Figure 21: Bending Moment Envelope Diagram for a 1.2m Thick Diaphragm Wall

Figure 22 shows that the maximum deflection observed in the revised design of the diaphragm wall is approximately 12% greater than that seen in the original design.

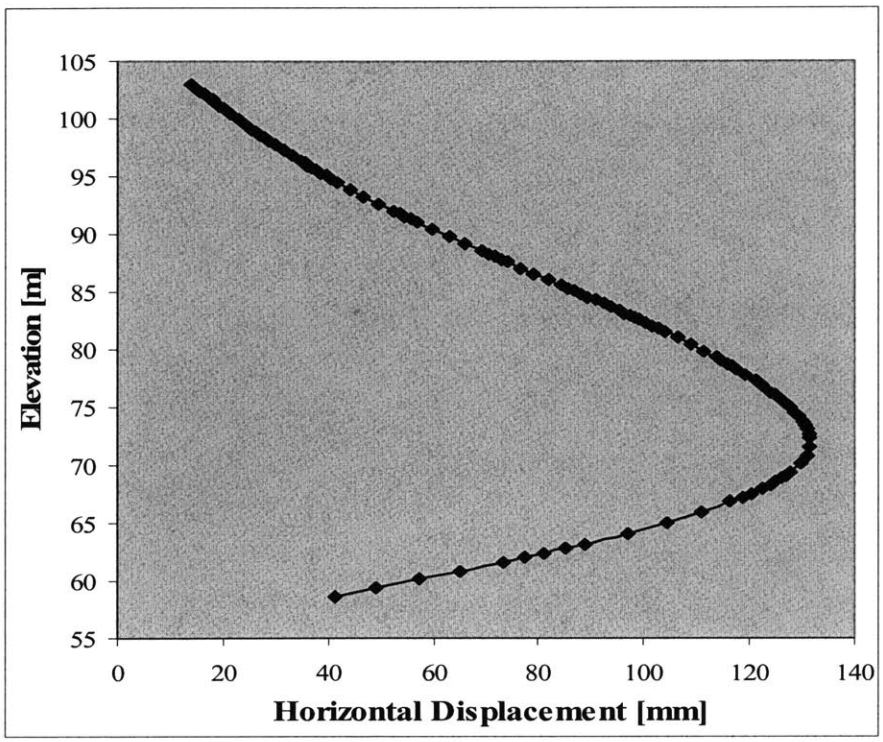

Figure 22: Maximum Deflection Diagram for a 1.2m Thick Diaphragm Wall

Although increasing the wall thickness is an effective design solution, Appendix H demonstrates that the additional cost for the Type M3 amounts to more than US$3 million. Alternative solutions to the proposed design might have included increasing the amounts of Jet Grout Piling (JGP) used in the design or embedding the concrete wall further into the Old Alluvium (embedment used was 3m).

5.3 Design of the Strutting System

For all practical purposes, struts in the excavation system behave like columns in a building. Hence, buckling was the greatest concern for the design of the strutting system. The effective or unbraced length in the x-x direction was nearly 10.1m. In the y-y direction this length was almost half (5.5m). The struts were braced to the king post at the middle of the excavation system on the x-x direction. Pre-loading forces were incorporated in the Plaxis model prior to installation of the struts in order to counteract the compression forces exerted by the soil and diaphragm wall on these members. The maximum observable axial forces in each stage of

the excavation were extracted from the Plaxis analysis. Since these forces only reflected one single line of struts, and the struts were spaced every 4m, the horizontal tributary area was factored into the calculations. These forces were fairly comparable to the ones observed in the original design. Please refer to Table 6 for a summary of the strutting system design and Table 7 for a summary of the original and revised Plaxis output strut reactions and strut member designs.

Strut	Section	Design Forces (KN)	Axial Capacities (KN)
1	W14x132	1981.0	3831.5
2	W14x132	1793.2	3831.5
3	W14x159	2897.9	4647.0
4	W14x159	2840.8	4647.0
5	W14x176	3016.5	5154.4
6	W14x176	3148.6	5154.4
7	W14x193	3442.0	5697.5
8	W14x176	3075.0	5154.4
9	W14x233	4137.1	6922.9
10	W14x145	2387.0	4216.6

Table 6: Summary of the Strutting System Design

Once the maximum axial forces were identified for each strut, a design was carried out using the AISC Manual of Steel Construction (ASD) Ninth Edition. The connections on each end of the struts were assumed (conservatively) to be pinned connections. Since the unbraced length on the x-x direction of the struts was greater, it was assumed to control the design. A check for slenderness ratios on each direction was later performed in order to confirm this assumption. All members were designed below 65% of their capacity to account for possible load increments in the removal stage of these members. Please refer to Appendix F for further detail on the strutting system design calculations.

Strut Layer	Max Strut Reaction Original Design (KN/m)	Max Strut Reaction Revised Design (KN/m)	Member Original Design	Member Revised Design
1	376	461	H-350	W14x132
2	831	848	H-400	W14x132
3	1249	1419	2H-400	W14x159
4	1249	1391	2H-400	W14x159
5	1263	1481	2HR-400	W14x176
6	1271	1549	H-414	W14x176
7	1402	1670	2H-400	W14x193
8	1493	1486	2H-414	W14x176
9	2173	2020	2H-400	W14x233
10	1400	1142	2HR-400	W14x145

Table 7: Summary of the Original and Revised Designs for the Strutting System

5.4 Design of Waler Connection

The waler connection was designed as per AASHTO Standard Specifications for Highway Bridges (14th Edition). The maximum strut load was used to design the strut-waler connection and the largest size strut was used for the waler beam. For practical purposes, all waler beams and stiffeners are to be the same size. As it was mentioned earlier, a major problem in the original design was the under-designed waler connections. The errors in their design caused the waler beams webs to fail in sway. The stiffener plates also failed in the original design. The effectiveness of incorporating channel sections instead of stiffener plates was not valid because, as previously explained, the small gain in axial load capacity came at expense of large decrements in the ductility of the waler connection. Consequently, it was decided that a proper design of the plate stiffeners would be sufficient to prevent vertical sway of the waler web section. In addition, the connection was changed to a single strut-waler connection as opposed to the splays used in the original design.

As per AASHTO specifications, the stiffener plates were designed as columns exposed to a compression load (strut axial force) and were therefore checked to resist buckling. Four stiffener plates were used in each waler connection (2 on each side of the waler beam web). A strip of web was incorporated in the cross-sectional area of the calculations. This strip had to be

equal to or less than the length contained between the stiffener plates plus 18 times the thickness of the waler beam web.

The waler section proposed is a W14x233 with four 1-in-thick stiffener plates spaced 12in from each other (6in from each side of the concentrated strut load). Please refer to Appendix G for further information on these calculations.

Figure 23 shows a plan and an elevation view of the revised design for the Diaphragm Wall, Strutting System and Waler Connection for the 9th level of struts. Other strut levels have the same waler connections but different strut member sizes.

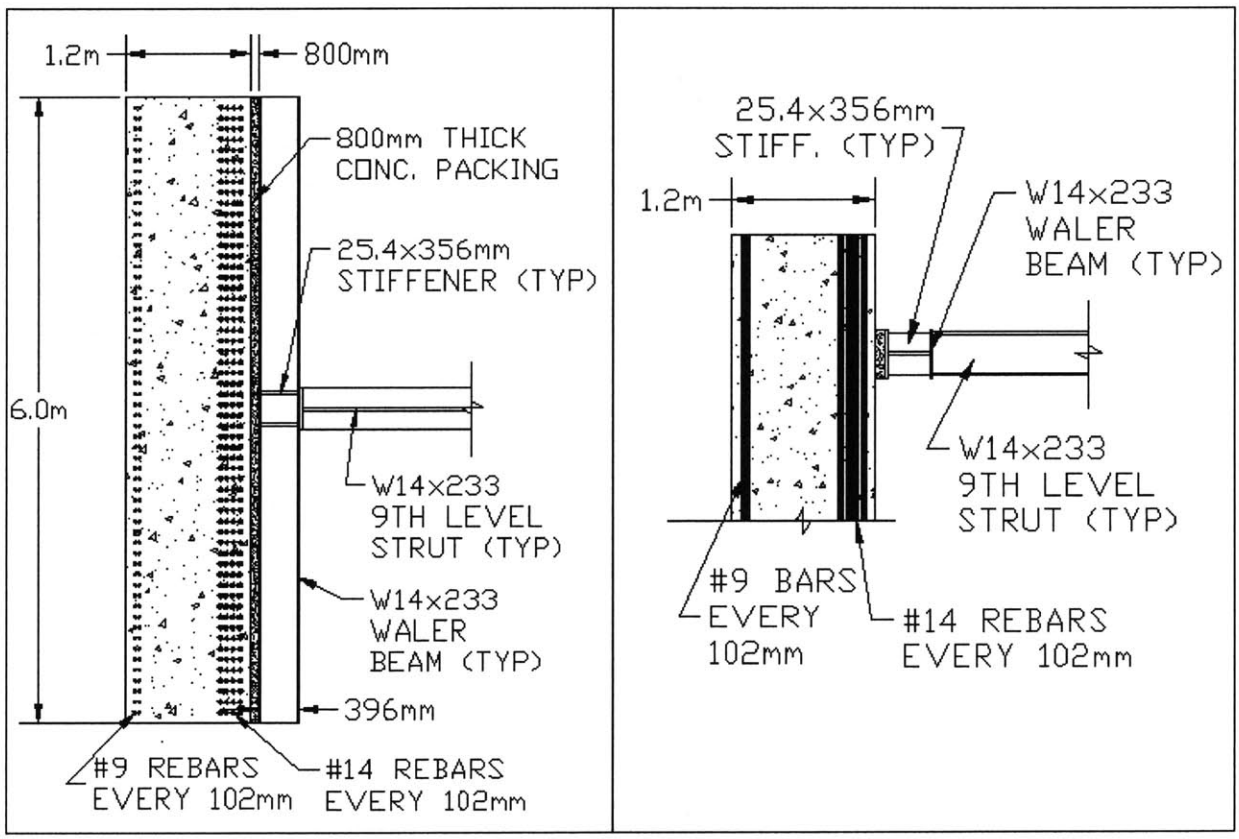

PLAN VIEW **ELEVATION VIEW**

Figure 23: Diaphragm Wall and Waler Connection Detail for the 9th Level of Struts.

6. Summary

Several valuable lessons arise from this thesis. Still, some of these lessons or recommendations should be used on a specific project basis. Each project must be appropriately assessed before considering these observations. In summary, these are the fundamental lessons that can be learned from this study:

1. An effective framework of hazard identification, consequential analysis, risk reduction strategies, and a responsive safety management should always be implemented in construction projects in order to identify and address any potential human errors and systems that may cause or contribute to a major catastrophe.
2. A large-scale deep excavation project has the potential to injure or to cause inconvenience to the public and must therefore be specially managed with careful instrumentation and monitoring.
3. There must be a continuous and visible commitment by management and workers, accompanied with an external consultative approach, to ensuring safety and health, from the inception of the design to the execution of the project.
4. New or unfamiliar technologies that are employed in the design of major elements of a construction project must be thoroughly evaluated and understood before they are adopted.

Finally, it is important to remember that most structural components are designed based on code calculations, and therefore have intrinsic redundancies built into them. These redundancies, in terms of their load bearing capacity, are over and above the various factors of safety applied in calculations of the capacity of each member. This robustness is a necessary and essential factor of safety and stability in the overall context of the design, and it should not be ignored.

7. References

American Association of State Highway and Transportation Officials. "Standard Specifications for Highway Bridges." Fourteenth Edition. 1989

American Institute of Steel Construction, Inc. "Manual of Steel Construction – Allowable Stress Design." Ninth Edition. 1989.

Architects Contractors Engineers. "Guide to Construction Costs." Thirty Fourth Edition. 2003

British Standard Code of Practice. "Earth Retaining Structures." (BS8002). BSI. 1994

Davies, Richard. "Report on Braced Excavation Collapse on 20th April 2004." Volume 1. July 2004

Konstantakos, Dimitrios. "Measured Performance of Slurry Walls." SMCEE Thesis, Massachusetts Institute of Technology, June 2000.

McCormac, Jack. "Structural Steel Design: ASD Method." Harper Collins Publishers, Inc. Fourth Edition. 1992.

Ministry of Manpower, Singapore (2005). "Report of the Committee of Inquiry into the Incident at the MRT Circle Line Worksite that Led to the Collapse of Nicoll Highway on 20th April 2004." May 17, 2005. http://www.mom.gov.sg/MOM/CDA

Nishimatsu Construction Co., Ltd. - Civil Engineering Design Department. "Study on Temporary Retaining Wall Type M-3." March 5, 2002.

Reed Construction Data. "Heavy Construction Cost Data." RSMeans. Eighteenth Edition. 2004

Xanthakos, Petros. "Slurry Walls as Structural Systems." McGraw-Hill, Inc. Second Ed. 1994

Whittle, Andrew. "Braced Excavation Collapse 20 April 2004 – Report on Geotechnical Aspects." Massachusetts Institute of Technology. July 2004

Whittle, Andrew. "Braced Excavation Collapse 20 April 2004 – Supplementary Report." Massachusetts Institute of Technology. January 18, 2005.

Appendix A: Original Design for the Diaphragm Wall

Summarized Plaxis Output Table (Original Model)

The following data was obtained from the Plaxis Analysis output in the original model: (Please note that this data gives the maximum forces/moments in each phase of the of the excavation and that the 21 phases in this model are comparable to the 24 phases used in the revised model)

Construction Phase	Max Deflections [mm]	Max Mom (+) [kNm/m]	Max Mom (-) [kNm/m]	Max. Shear [kN/m]
1	51.2	203.6	-107.4	-243.0
2	26,3	272.4	-101.9	-240.0
3	54.3	769.6	-220.5	309.9
4	46.8	680.5	-340.3	350.5
5	75.3	1101.4	-528.6	552.3
6	65.2	857.0	-400.9	487.3
7	90.1	1294.8	-1150.5	825.8
8	82.7	1111.6	-529.1	510.5
9	106.5	1596.2	-852.9	918.5
10	97.1	1335.2	-581.9	544.9
11	114.1	1701.1	-621.3	920.2
12	105.3	1401.1	-579.6	534.2
13	117.6	1783.4	-725.2	937.4
14	107.7	1305.4	-652.6	507.1
15	114.6	1632.0	-760.8	922.9
16	107.6	987.5	-652.2	-465.6
17	107.6	885.8	-513.2	806.0
18	107.4	883.8	-512.0	-591.0
19	106.8	1050.4	-1240.1	1247.0
20	107.0	878.9	-783.2	836.3
21	107.0	1325.6	-1078.2	997.5
Overall Maximum	**117.6**	**1783.4**	**-1240.1**	**1247.0**

Diaphragm Wall Design of Main Rebars

Please note that envelope calculations for the moments were included in this design, thereby leading in some occasions to greater moments than those shown in the summarized Plaxis output table for the original model.

Design Data:

f_{cu}	=	40 N/mm^2	f_c	=	18 N/mm^2
f_y	=	460 N/mm^2	f_{sy}	=	400 N/mm^2
B	=	6000 mm	γ_{ms}	=	1.15 mm
h	=	800 mm	γ_{LF}	=	1.2 mm

Reinforcement Against (+) Moment

Level [m bgl]	d [mm]	K	Mmax KNm/m	Reqr'd As mm^2	**Provided As mm^2**
7.8	710	0.912	1209	5601.371	**5864.30**
12.8	710	0.889	1369	6506.757	**6597.35**
30.8	710	0.862	1795	8798.732	**9617.47**
37.3	710	0.925	1050	4796.346	**5864.30**
44.3	710	0.903	1326	6204.670	**6597.35**

Reinforcement Against (-) Moment

Level [m bgl]	d [mm]	K	Mmax KNm/m	Reqr'd As mm^2	**Provided As mm^2**
5.3	710	0.916	1162	5360.1	**5864.30**
11.8	710	0.826	2170	11100.5	**11728.62**
19.3	710	0.944	800	3580.8	**3753.15**
24.3	710	0.872	1692	8198.7	**8796.47**
34.3	710	0.91	1240	5757.6	**5864.30**
44.3	710	0.947	761	3395.5	**3753.15**

Appendix B: Original Design for the Strutting System

Strutting System Design

Axial Loads: (Please refer to Plaxis output for more information)

Strut	1	2	3	4	5	6	7	8	9	10
Pre-load Force	200	550	650	600	700	700	800	850	800	700
Phase 1	0	0	0	0	0	0	0	0	0	0
Phase 2	200	0	0	0	0	0	0	0	0	0
Phase 3	376	0	0	0	0	0	0	0	0	0
Phase 4	23	550	0	0	0	0	0	0	0	0
Phase 5		831	0	0	0	0	0	0	0	0
Phase 6		423	650	0	0	0	0	0	0	0
Phase 7		205	1249	0	0	0	0	0	0	0
Phase 8		358	667	600	0	0	0	0	0	0
Phase 9		313	521	1249	0	0	0	0	0	0
Phase 10		351	604	648	700	0	0	0	0	0
Phase 11		357	548	560	1263	0	0	0	0	0
Phase 12		351	601	594	692	700	0	0	0	0
Phase 13		353	601	529	637	1271	0	0	0	0
Phase 14		347	607	593	651	643	800	0	0	0
Phase 15		343	616	590	592	564	1402	0	0	0
Phase 16		337	609	596	652	626	734	850	0	0
Phase 17		336	614	603	653	588	610	1493	0	0
Phase 18		333	612	599	656	622	688	879	800	0
Phase 19		333	616	605	666	622	588	765	2173	0
Phase 20		329	615	604	663	624	629	807	1649	700
Phase 21		329	618	607	667	632	632	732	1630	1400
MAX Values (KN/m)	**376**	**831**	**1249**	**1249**	**1263**	**1271**	**1402**	**1493**	**2173**	**1400**

Summary Table

Strut Layer	Max Strut Reaction Original Design (KN/m)	Max Strut Reaction Revised Design (KN/m)	Member Original Design	Member Revised Design
1	376	461	H-350	W14x132
2	831	848	H-400	W14x132
3	1249	1419	2H-400	W14x159
4	1249	1391	2H-400	W14x159
5	1263	1481	2HR-400	W14x176
6	1271	1549	H-414	W14x176
7	1402	1670	2H-400	W14x193
8	1493	1486	2H-414	W14x176
9	2173	2020	2H-400	W14x233
10	1400	1142	2HR-400	W14x145

As it can be observed from the summary table above, there is not much difference between the strut forces in each model (original and revised). Hence, the designs of the strutting system members under each model should be approximate.

However, due to the incorporation of removal phases in the original excavation design, the strut forces used in this design increased by as much as 70% in some levels. The revised design does not include these phases and therefore cannot compare to these values. A table including all three sets of values is shown below.

Strut Layer	Max Strut Reaction in Original Design Including Excavation Phases Only (KN/m)	Max Strut Reaction in Original Design Including Removal Phases (KN/m)	Max Strut Reaction Revised Design (KN/m) (Excavation Phases Only)
1	376	568	461
2	831	1018	848
3	1249	1816	1419
4	1249	1635	1391
5	1263	1459	1481
6	1271	1322	1549
7	1402	2130	1670
8	1493	2632	1486
9	2173	2173	2020
10	1400	1400	1142

The sizes of the strut members used in the original design can be seen in Appendix B of the thesis.

Appendix C: Original Design for the Waler Connection

H-400 (HR-400)
Check Web Buckling And Bearing Resistance {Ref: BS5950:Part 1:1990}
{Not applicable for angles.}

.i) Design Data: {Input data are shown boxed.}
.i.1) Design Force:
Factored reaction load F_x = [ ] kN at end of beam.
Factored reaction load F_x = [2796.0] kN at interior of beam
.i.2) Trial Steel Section: [H-400x400x13x21]
.i.3) Steel strength: p_Y = [265] N/mm^2
.i.4) Properties of section:

A =	218.7 cm^2	t_w =	13 mm	d =	314 mm	{D - 2(t_f + r)}
D =	400 mm	t_f =	21 mm	w_t =	172 kg/m	
B =	400 mm	r =	22 mm			

.i.5) $\lambda = 2.5*d/t_w$ = 60.3846

.ii) Buckling resistance of the unstiffened web:
.ii.1) Compressive strength p_c = 213.231 N/mm^2

.ii.2) Check at end of beam
Stiff bearing length b1 = [ ] mm {e.g., bearing plate, end of strut, etc.}
$\eta 1 = 0.5*D$ = N/A mm
Buckling resistance $P_w = (b1+\eta 1)t_w p_c$ = N/A O.K.!

.ii.3) Check at interior of beam
Stiff bearing length b1 = [400] mm {e.g., bearing plate, end of strut, etc.}
$\eta 1 = 0.5*D*2$ = 400 mm
Buckling resistance $P_w = (b1+\eta 1)t_w p_c$ = 2217.6 kN < Fx N.G.? Provide stiffeners.

∴ Web stiffener plates required.

.iii) Bearing check of the unstiffened web
Required $A_{br} \geq F_x/p_y$ = N/A mm^2 at end of beam.
Required $A_{br} \geq F_x/p_y$ = 10550.9 mm^2 at interior of beam.
.iii.1) Check at end of beam
Actual $A_{br} = [b1 + 2.5(t_f + r)]*t_w$ = N/A mm^2 O.K.!
.iii.2) Check at interior of beam
Actual $A_{br} = [b1 + 5(t_f + r)]*t_w$ = 7995.0 mm^2 N.G.? Provide stiffeners.

∴ Web stiffener plates required to increase bearing area.

Developed by: DPMundo

UserID: Nishimatsu Const. Co., Ltd.

Source : E72 Pg 74-10

Figure 5.6	Design calculations for waler connection showing the error in stiff bearing length (extract from E72).

4.5 Check against web buckling and bearing

· Design load

The factored strut reaction (Nu) in below table are derived from P.4~25.

Waler Member	Strut	Factored max. force in one strut member Nu (kN/No)	Max. Bearing load Pbr (kN/No)	TYPE*	Stiffener Plate (mm)
H-294H-300, HR-300	Single	1979	1979	1	*1 2×12
H-344		2799	2799		
H-350, HR-350		2204	2204		
H-350 (M1-1*, M3-1*)		2891	2891		*2 4×12
H-400, HR-400		5592	2796	2	*1 2×12
HR-400 (S-1*)		3630	3630	1	*2 4×12
H-400, HR-400	Double	5314	3543	3	
H-414	Single	8784	4392	2	*1 2×12
H-414	Double	6439	4293	3	

* refer to the sketch below

Considering the effect of splays, the bearing load Pbr is derived as follows:

For single strut (TYPE-1)

Pbr = Nu / 2

For double struts (TYPE-2)

Pbr = 2Nu / 3

*1 : Stiffener plates at Top & Bottom

*2 : Double stiffener plates at Top & Bottom

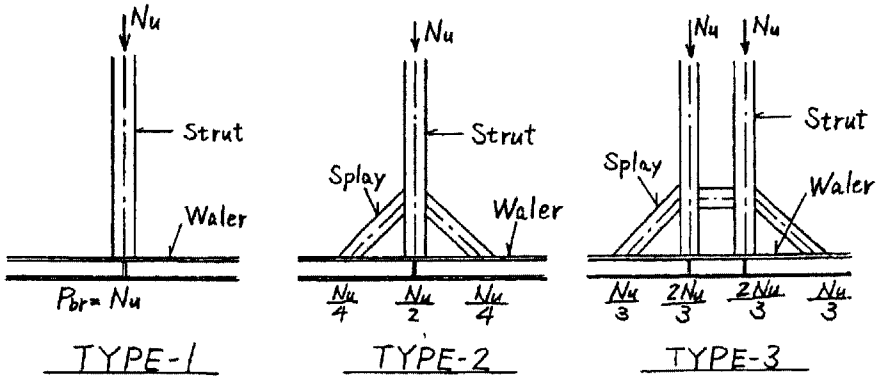

Note: Required stiffener plates to be provided at the connection between waler and main strut only.

The calculation results are shown in P. 74-2 ~ 74-19.

Source : E72 Pg 74-1

Figure 5.7 Design calculation for waler connections (extract from E72).

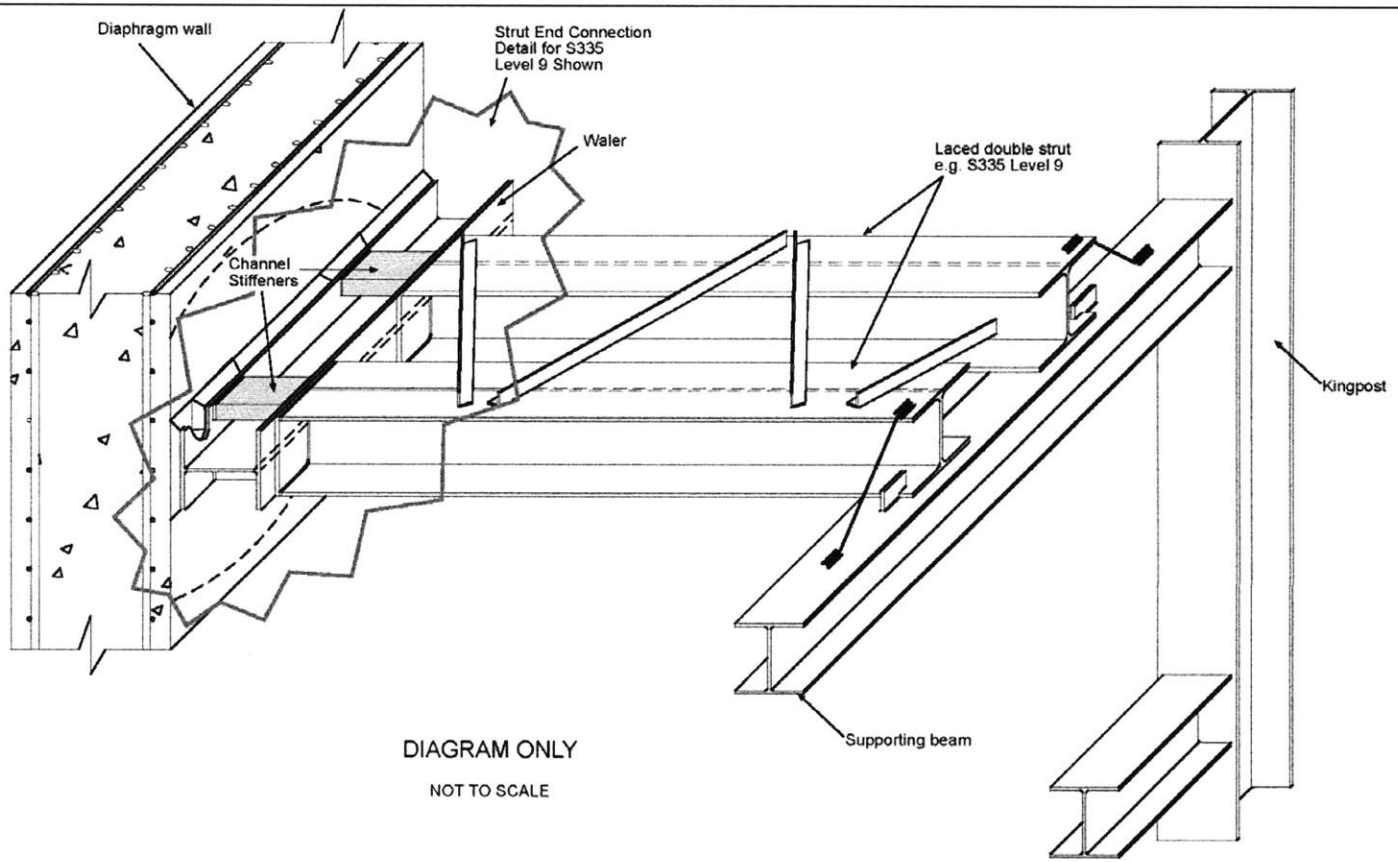

Source : Aviva ER Fig 19

Figure 5.9	The arrangement of strutting system at S3359 including the arrangement of the C-channel in the waler.

TEMPORARY WORKS-DRAWING CHANGE NOTIFICATION

NLC JV		CONTRACT:	Circle Line Stage 1 C824
Date:	18/Feb/2014	Prepared By:	T. Shimizu
Drawing Change Notification Number:	DCN/824/NCH/		
The Change of Stiffener plate			
Drawing Number:	W/824/ CVB/DET/2225	Revision:	

The Changes will be Incorporated into:	1. Same Drawing New Revision:	
	2. As Built Drawing – Same Number:	✓
	3. New Drawing:	

Description of Amendment:

The change of stiffener plate.

original revise

12mm thk. plate ⇒ [-200×80 ([-150×75)

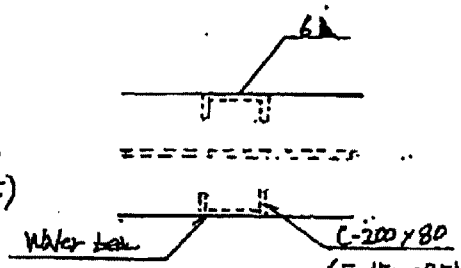

Attached Sketch(es) Number:	

Reason for Amendment:

Because of material.

Other Remarks/Comments:

Approval Status	Approved	Not Approved - Reason	Sign	Date
NLC Design Manager	✓			27/Feb/14
NLC Temp Works PE	✓			27/02/14

Pls refer to attached calculation paper for the application of each channel member as a stiffener member.

Source : Maunsell ER Pg 82

Figure 5.10	Temporary Works – Drawing Change Notification for change from stiffener plates to C-channel.

Design of Web Stiffeners against Web Buckling

Waler Member	Strut	Factored reaction load F_x (kN)*	Buckling resistance P_w (kN)*	$F_x - P_w$ (kN)	TYPE
H-400, HR-400	Single	2796	2218	578	1
	Double	3543		1325	2
H-414	Single	4392	3500	892	2
	Double	4293		793	2

* refer to C824/DES/CA/0104D P. 74-10, 74-14, 74-16, 74-18

(1) TYPE－1

Provide 2[-150×75×6.5×10

$A=2\times23.71=47.42cm^2$

$r_x=6.08cm$

$r_y=2.22cm$

$L_e=41.4-2\times2.8=35.8cm$

$\lambda_x=L_e/r_x=5.9$, $\lambda_y=L_e/r_y=16.1$

$p_c=264N/mm^2$ (BS5950 Table27(c))

$P_c=pc\cdot A=264\times47.42\times10^2=1252kN > F_x-P_w=578kN$ OK!

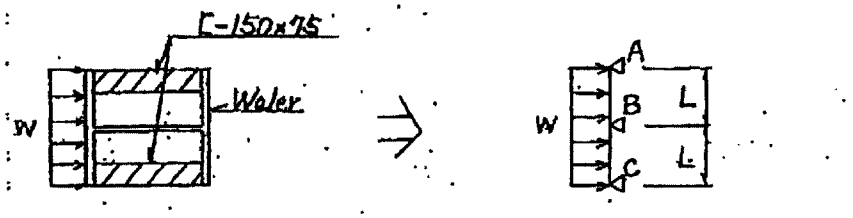

$R_A=R_C=0.375wL$

$R_B=1.25wL$

・2[-150×75×6.5×10

$R_A+R_C=0.375\times2796=1049kN < P_c=1252kN$ OK!

・Web

$R_B=1.25\times2796/2=1748kN < P_w=2218kN$ OK!

Source : Maunsell ER Pg 83

Figure 5.11(a)	Design calculations for C-channel connection in Drawing Change Notification.

(2) TYPE－2

Provide 2[-200×80×7.5×11

$A=2\times31.33=62.66cm^2$

$r_x=7.88cm$

$r_y=2.32cm$

$L_e=40.0-2\times2.1=35.8cm$

$\lambda_x=L_e/r_x=4.5$, $\lambda_y=L_e/r_y=15.4$

$p_c=265N/mm^2$ (BS5950 Table27(c))

$P_c=pc \cdot A=265\times62.66\times10^2=1660kN > F_x-P_w=1325kN$ OK!

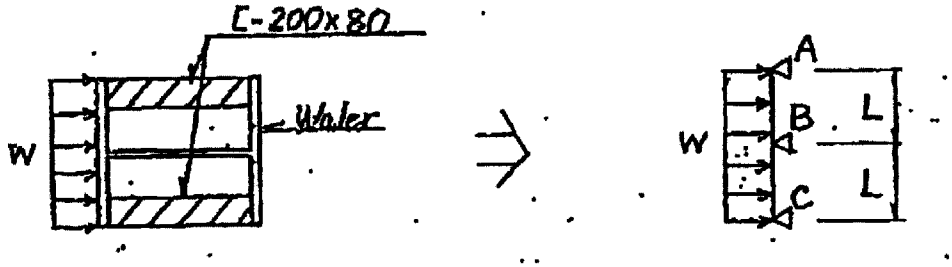

$R_A=R_C=0.375wL$

$R_B=1.25wL$

・2[-200×80×7.5×11

$R_A+R_C=0.375\times4392=1647kN < P_c=1660kN$ OK!

・Web

$R_B=1.25\times4392/2=2745kN < P_w=3500kN$ OK!

Source : Maunsell ER Pg 84

Figure 5.11(b)	Design calculations for C-channel connection in Drawing Change Notification.

Appendix D: Plaxis Output/Revised Analysis

Summarized Plaxis Output Table (Revised Model)

The following data was obtained from the Plaxis Analysis output in the revised model: (Please note that this data gives the maximum moments in each phase of the of the excavation and that the 24 phases in this model are comparable to the 21 phases used in the original model)

Construction Phase	Max Deflections [mm]	Max Mom (+) [kNm/m]	Max Mom (-) [kNm/m]
1	2.99	10.3	13
2	2.99	10.4	13
3	7.78	152	167
4	46.3	-	587
5	23.75	637.6	557.5
6	44.59	1900.8	1135
7	39.95	1764.2	1022.9
8	57.53	2799	1411
9	54.17	2600	1357
10	71	3635.8	1896
11	67.18	3350	1808
12	86.1	4471	2222
13	81.62	4150	2080
14	99.46	5026	1452.3
15	95.63	4670	1375.4
16	113.9	5410	1452.3
17	110.3	4950	1313.4
18	123.3	5400	1177.8
19	119.68	4800	1131.7
20	125.9	5440	1233.4
21	123	5160	1102.7
22	130.98	6210	1236.6
23	128.4	5730	1243.5
24	131.6	5920	1244
Overall Maximum	**131.6**	**6210.0**	**13.0**

Plaxis Output Table (Revised Model)

The following data was obtained from the Plaxis Analysis output: (Please note that this data gives the force envelope including all the phases of the of the excavation)

Elevation	Max Deflections	Max Mom (+)	Max Mom (-)	Max. Shear (+)	Max. Shear (-)
[m]	[mm]	[kNm/m]	[kNm/m]	[kN/m]	[kN/m]
102.9	14.10	0.00	0.00	0.29	-0.63
102.65	14.85	0.41	-1.26	3.81	-10.02
102.4	15.59	1.95	-5.00	8.70	-19.84
102.15	16.34	4.72	-11.18	13.55	-29.58
101.9	17.08	8.68	-19.78	17.90	-39.28
101.9	17.08	8.68	-19.78	422.17	-292.47
101.65	17.82	84.48	-91.46	412.05	-301.99
101.4	18.57	186.21	-168.35	401.46	-313.13
101.15	19.31	285.22	-248.13	390.39	-325.04
100.9	20.05	381.37	-330.94	378.87	-337.70
100.9	20.05	381.37	-330.94	379.01	-337.53
100.45	21.40	547.13	-488.12	357.74	-361.49
100	22.77	703.16	-656.54	335.34	-387.22
99.55	24.15	848.81	-836.98	311.65	-414.85
99.1	25.56	983.43	-1030.21	286.52	-444.48
99.1	25.56	983.43	-1030.21	582.27	-72.54
98.875	26.28	1046.44	-1035.54	575.85	-88.28
98.65	27.01	1106.52	-1057.20	569.56	-104.11
98.425	27.75	1163.65	-1082.40	563.40	-119.86
98.2	28.49	1217.83	-1111.11	557.38	-135.37
98.2	28.49	1217.83	-1111.11	556.77	-137.50
97.75	30.00	1318.86	-1182.81	541.09	-181.40
97.3	31.54	1410.53	-1274.57	524.93	-226.62
96.85	33.12	1492.79	-1387.05	508.36	-273.46
96.4	34.73	1565.63	-1520.97	491.40	-322.24
96.4	34.73	1565.63	-1520.97	491.64	-321.82
96.2	35.46	1595.48	-1587.56	484.99	-344.31
96	36.20	1623.91	-1658.74	478.14	-367.36
95.8	36.95	1650.93	-1734.58	471.11	-391.01
95.6	37.70	1676.51	-1815.18	463.91	-415.27
95.6	37.70	1676.51	-1815.18	1158.37	-0.34
95.35	38.67	1706.49	-1691.86	1128.41	-0.33
95.1	39.65	1734.25	-1576.40	1097.67	-0.33
94.85	40.64	1759.79	-1469.05	1066.21	-0.32
94.6	41.65	1783.10	-1374.17	1034.03	-0.32
94.6	41.65	1783.10	-1374.17	1034.14	-0.32
93.975	44.21	1885.96	-1312.46	950.63	-0.31
93.35	46.85	2105.09	-1308.92	862.75	-95.96
92.725	49.55	2294.34	-1366.92	770.50	-199.10
92.1	52.32	2453.45	-1489.85	673.92	-307.91
92.1	52.32	2453.45	-1489.85	1389.77	-4.01
91.85	53.46	2508.58	-1356.32	1347.49	-5.19
91.6	54.61	2558.92	-1271.64	1304.53	-13.59
91.35	55.77	2604.42	-1198.54	1260.93	-21.98
91.1	56.94	2645.04	-1137.29	1216.72	-30.37
91.1	56.94	2645.04	-1137.29	1216.61	-30.37
90.475	59.89	2827.27	-1037.22	1103.15	-51.38
89.85	62.89	3077.37	-1015.69	985.21	-72.52

89.225	65.92	3280.84	-1076.20	862.75	-202.15
88.6	68.99	3437.17	-1222.27	735.71	-344.28
88.6	68.99	3437.17	-1222.27	1502.50	-115.03
88.35	70.25	3486.91	-1020.86	1447.33	-123.43
88.1	71.51	3529.26	-833.84	1391.41	-131.70
87.85	72.78	3564.31	-733.42	1334.86	-139.78
87.6	74.05	3592.16	-652.02	1277.76	-147.63
87.6	74.05	3592.16	-652.02	1277.69	-147.05
87.1	76.59	3748.30	-535.45	1161.74	-162.13
86.6	79.14	3948.30	-481.95	1043.43	-175.46
86.1	81.69	4108.81	-492.99	923.32	-186.43
85.6	84.23	4231.47	-570.03	801.94	-220.76
85.6	84.23	4231.47	-570.03	1649.17	-206.17
85.35	85.52	4281.13	-359.40	1586.58	-204.96
85.1	86.80	4324.58	-165.05	1523.92	-203.34
84.85	88.08	4362.10	-136.83	1460.90	-201.58
84.6	89.36	4393.93	-142.79	1397.26	-200.00
84.6	89.36	4393.93	-142.79	1396.77	-200.36
84.3	90.88	4424.90	-149.22	1320.65	-198.17
84	92.39	4448.42	-155.07	1242.97	-197.70
83.7	93.88	4464.00	-160.74	1162.69	-199.75
83.4	95.37	4583.58	-166.62	1078.75	-205.11
83.4	95.37	4583.58	-166.62	1077.39	-207.09
83.2	96.34	4659.18	-171.12	1022.71	-215.10
83	97.32	4727.67	-175.98	966.78	-226.85
82.8	98.28	4789.00	-181.17	909.92	-242.86
82.6	99.24	4843.14	-186.65	852.42	-258.84
82.6	99.24	4843.14	-186.65	1699.14	-258.66
82.35	100.44	4901.06	-193.90	1622.14	-278.22
82.1	101.63	4947.83	-201.58	1544.62	-297.37
81.85	102.80	4983.69	-209.67	1466.63	-316.07
81.6	103.96	5008.88	-218.16	1388.27	-334.29
81.6	103.96	5008.88	-218.16	1388.19	-334.39
81.025	106.56	5026.95	-239.24	1206.70	-375.14
80.45	109.06	5190.91	-262.50	1022.91	-414.26
79.875	111.45	5331.60	-288.01	836.87	-451.88
79.3	113.73	5401.64	-315.85	648.64	-489.68
79.3	113.73	5401.64	-315.85	1384.64	-489.55
79.05	114.72	5410.84	-328.69	1298.44	-517.07
78.8	115.68	5407.07	-342.00	1211.85	-544.54
78.55	116.62	5390.54	-355.78	1124.92	-572.44
78.3	117.54	5361.44	-370.02	1037.68	-600.17
78.3	117.54	5361.44	-370.02	1037.60	-600.44
77.8	119.31	5329.85	-399.91	862.02	-654.59
77.3	120.98	5394.25	-462.22	684.90	-708.68
76.8	122.56	5396.99	-601.84	506.36	-761.85
76.3	124.05	5338.80	-745.72	326.49	-813.23
76.3	124.05	5338.80	-745.72	1765.90	-811.62
76.05	124.79	5287.85	-819.16	1671.15	-837.69
75.8	125.51	5221.53	-893.26	1576.18	-861.85
75.55	126.20	5140.42	-967.04	1481.05	-884.92
75.3	126.85	5045.09	-1039.42	1385.81	-907.75
75.3	126.85	5045.09	-1039.42	1385.72	-905.70
74.925	127.78	4917.74	-1172.56	1242.53	-713.45
74.55	128.62	4949.01	-1243.32	1098.69	-521.84
74.175	129.37	5049.21	-1257.19	954.22	-349.38
73.8	130.02	5359.47	-1235.32	809.16	-221.55

73.8	130.02	5359.47	-1235.32	1419.99	-263.59
73.425	130.60	5635.46	-1211.67	1268.60	-314.39
73.05	131.06	5856.59	-1195.35	1116.42	-365.27
72.675	131.40	6022.41	-1186.26	963.48	-415.34
72.3	131.61	6132.43	-1184.34	809.83	-464.82
72.3	131.61	6132.43	-1184.34	809.66	-466.55
71.575	131.58	6212.23	-1279.09	510.00	-558.01
70.85	130.96	6133.53	-1423.47	206.41	-657.77
70.125	129.72	5915.24	-1605.07	17.59	-774.51
69.4	127.85	5728.53	-1925.53	9.77	-891.74
69.4	127.85	5728.53	-1925.53	13.80	-865.91
69.125	126.98	5623.42	-2060.26	35.78	-756.79
68.85	126.03	5538.29	-2155.60	71.20	-642.66
68.575	125.00	5470.80	-2209.95	123.05	-523.24
68.3	123.89	5418.71	-2222.04	179.46	-402.76
68.3	123.89	5418.71	-2222.04	179.47	-414.47
67.925	122.24	5374.09	-2175.21	283.04	-244.62
67.55	120.45	5367.35	-2062.98	375.40	-96.16
67.175	118.51	5392.78	-1905.28	463.86	-0.14
66.8	116.43	5441.61	-1722.67	499.34	-0.14
66.8	116.43	5441.61	-1722.67	487.19	-0.13
65.9	110.80	5405.68	-1326.73	392.57	-228.29
65	104.29	5116.69	-1015.88	299.07	-475.79
64.1	96.96	4578.69	-787.10	209.48	-734.96
63.2	88.88	3796.97	-636.64	126.57	-1000.14
63.2	88.88	3796.97	-636.64	135.30	-976.65
62.8	85.08	3395.97	-634.37	120.35	-1027.23
62.4	81.18	2976.24	-639.60	106.96	-1070.14
62	77.18	2540.43	-646.29	96.82	-1107.22
61.6	73.10	2090.96	-652.18	91.60	-1140.31
61.6	73.10	2090.96	-652.18	103.76	-1093.60
60.85	65.29	1341.93	-669.50	191.32	-868.14
60.1	57.34	805.55	-506.39	319.95	-605.57
59.35	49.31	399.09	-236.50	384.80	-480.14
58.6	41.23	0.00	0.00	185.31	-666.11
Overall Maximum	**131.61**	**6212.23**	**-2222.04**	**1765.90**	**-1140.31**

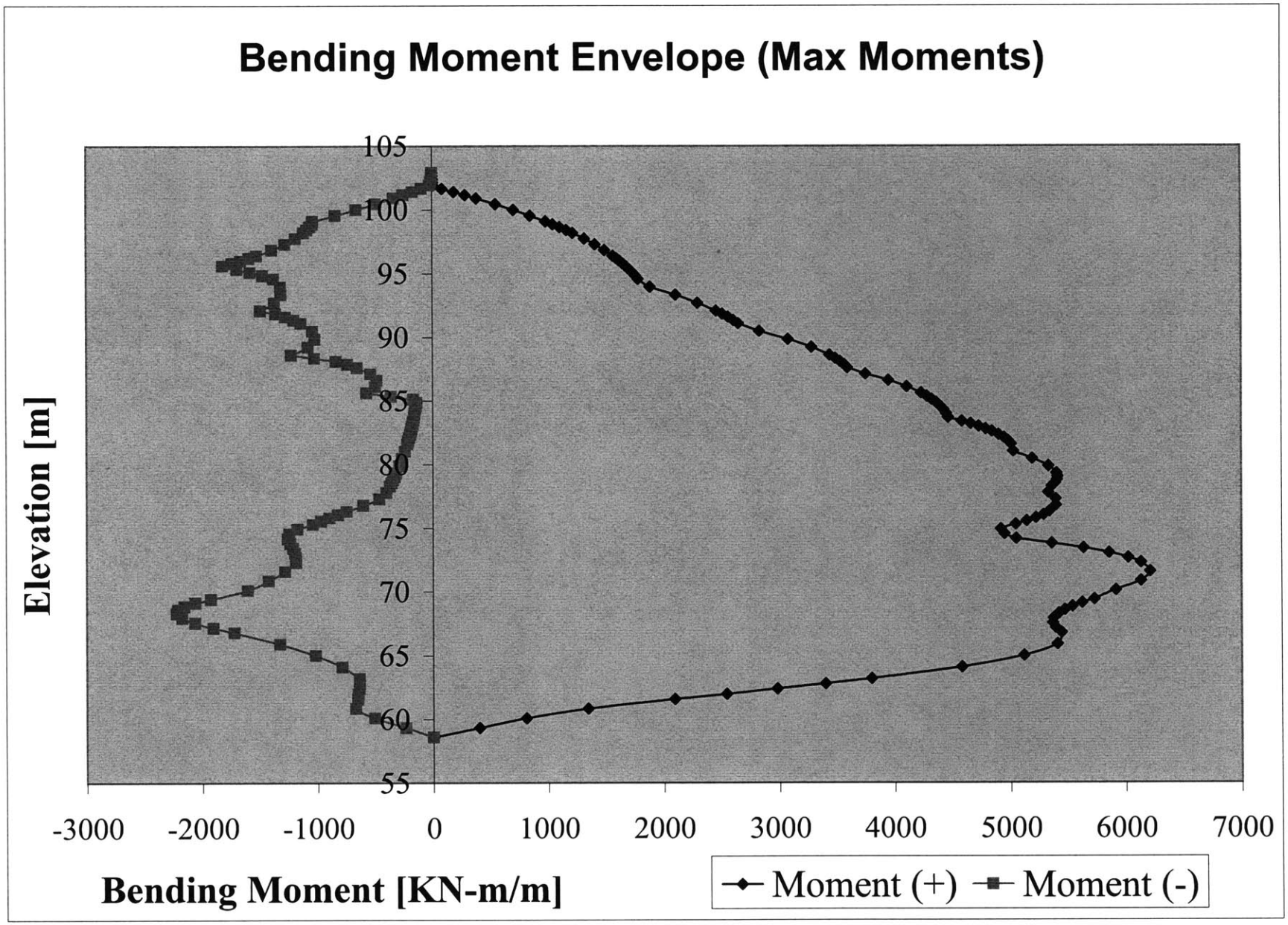
Bending Moment Envelope (Max Moments)
Elevation [m]
105
100
95
90
85
80
75
70
65
60
55
-3000
-2000
-1000
0
1000
2000
3000
4000
5000
6000
7000
Bending Moment [KN-m/m]
Moment (+)
Moment (-)

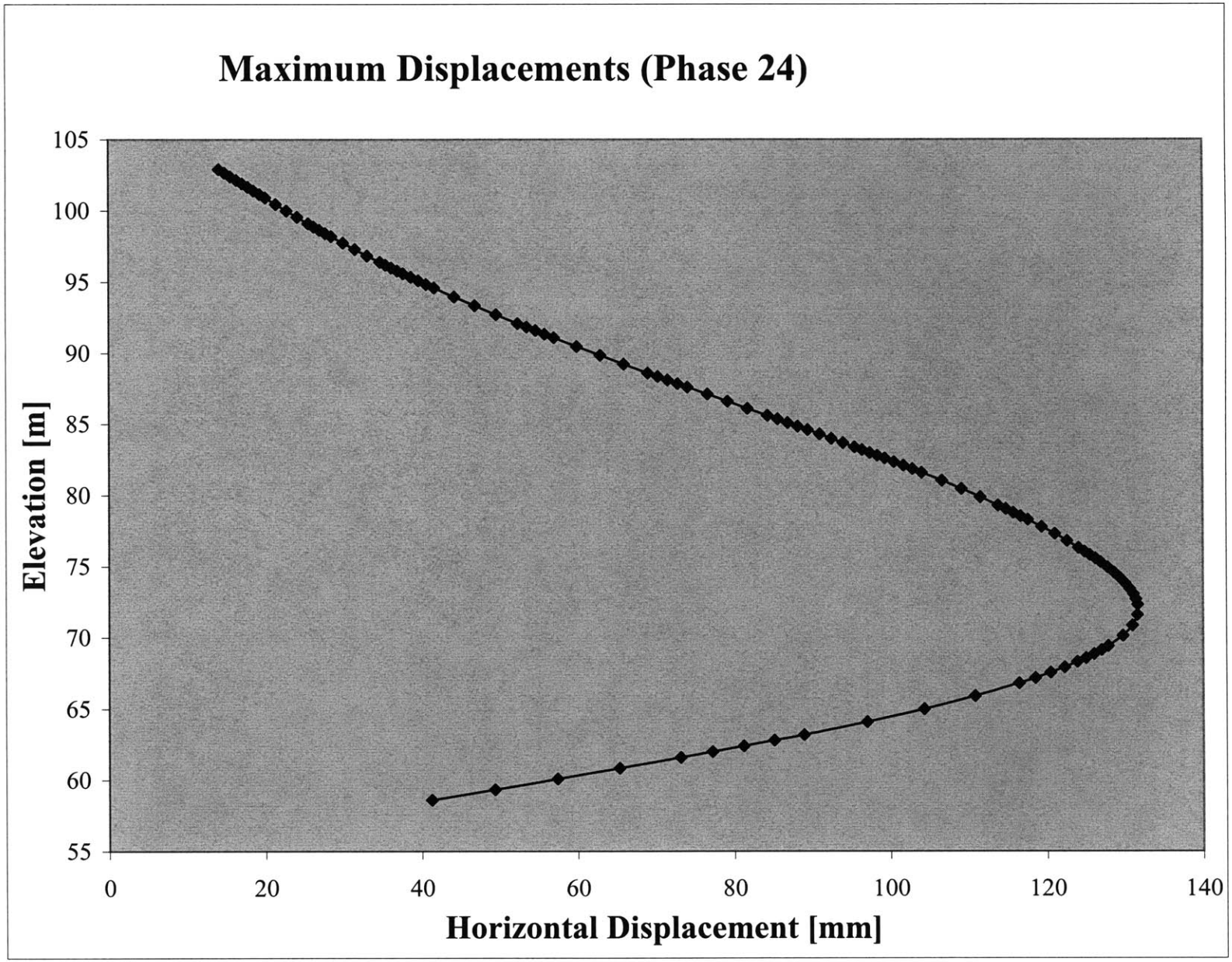
Maximum Displacements (Phase 24)
Elevation [m]
105
100
95
90
85
80
75
70
65
60
55
0
20
40
60
80
100
120
140
Horizontal Displacement [mm]

Appendix E: Proposed Design for the Diaphragm Wall

Diaphragm Wall Design

Conversion Values

1 KN	=	0.224809	kips
1 MPa	=	0.145038	ksi
1 m	=	3.28084	ft

Plaxis Analysis Output Values (Force Envelopes)

Maximum Moment (+)	=	6.21	MN-m/m	=	**1396 k-ft/ft**
Maximum Moment (-)	=	2.22	MN-m/m	=	**499 k-ft/ft**
Negative Rebar Depth (Top)	=	17.3	m	=	**56.8 ft**
Negative Rebar Depth (Bottom)	=	19.9	m	=	**65.3 ft**
Maximum Axial Force (P)	=	727	KN/m	=	**50 k/ft**

Transverse Steel Reinforcement

Rebar design as per AASHTO Standards

Notes and Assumptions:
English System was adopted for these calcualtions. Converted values to Metric System are shown in thesis
All calculations are done per foot of length of wall
Please refer to Plaxis output for further information on the analysis

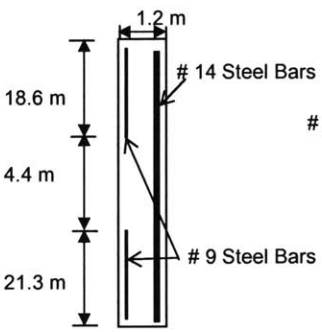

Wall Elevation
NTS

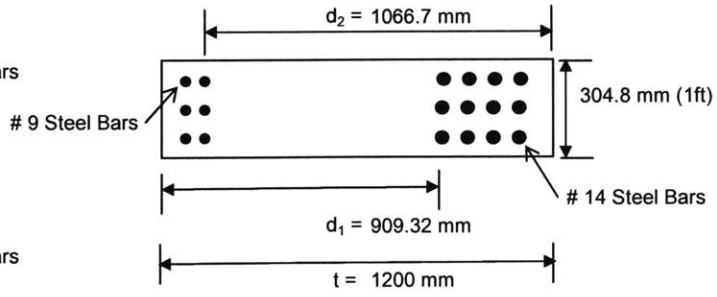

Wall Plan
NTS

Reinforcement at near-end of diaphragm wall (positive moment):

INPUT VALUES

Use grade 60 steel reinforcing bars

Es	=	29000	ksi		
Ec	=	5000	ksi		
fy	=	60	ksi		
f'c	=	4	ksi		
cover length	=	3	in		
Width (b)	=	12	in		
Wall Thickness	=	**1.2**	**m**	**=**	**47.2 in**

Choose Bar Size # : **14**

Bar diameter	=	1.690	in	
Bar spacing	=	4	in	**OK>1.5*db**
Number of rows	=	4		

OUTPUT VALUES

Wall Section Properties:

EA	=	4.14E+07 KN/m	
EI	=	4.96E+06 KN m^2/m	

Loads/Moments obtained from Plaxis analysis:

Positive Bending Moment (M_{wall})	=	1396 k-ft / ft of wall	(Absolute value)
Max. Axial Force (P)	=	50 k / ft of wall	(Compression)

Check Cracking Moment (M_{crack}): AASHTO 8.13.3

Depth (d_1)	=	35.8 in	
xbar (from left)	=	23.6 in	
$I_g = b*(t_{bott}^3)/12$	=	105449 in^4	
y_t	=	23.6 in	(Distance from N.A to edge in tension)
fr	=	0.5 ksi	AASHTO 8.15.2.1.1
$M_{crack} = f_r*I_g / y_t$	=	176 k-ft	
$1.2*M_{crack}$	=	212 k-ft	AASHTO 8.17.1.2

Required Area of Reinforcing Steel:

fs	=	24 ksi	
fc	=	1.6 ksi	
n = Es/Ec	=	6	
r = fs/fc	=	15	
k = n/(n+r)	=	0.28	
j = 1-k/3	=	0.91	
d_1-xbar	=	12.2 in	
$M_a = M_{wall} + P*(d_1\text{-xbar})$	=	1447 k-ft / ft of wall	**Ma>1.2*Mcrack**
Design Moment (M_d)	=	**1447** k-ft / ft of wall	
Reqr'd As = $[M_d/(fs*j*d_1) - P/(fs)]$	=	20.20 in^2 / ft of wall	
Actual A_s (per ft)	=	**26.92** in^2 / ft of wall	**OK > reqr'd**

Note:

Due to a varying moment, # 14 bars spaced every 4-in might not be needed for the entire depth of the wall. However, because significant depth of the wall would need this amount of reinforcement, it was assumed that these rebars would run the entire depth of the wall. Please refer to Plaxis output for more information on the moment diagram of the diaphragm wall.

Reinforcement at far-end of diaphragm wall (negative moment):

INPUT VALUES

Choose Bar Size # :		9	
Bar diameter	=	1.125 in	
Bar spacing	=	4 in	**OK>1.5*db**
Number of rows	=	2	

OUTPUT VALUES

Negative Bending Moment (M_{wall})	=	499 k-ft / ft_{wall}	
P (Axial Force of Wall)	=	50 k / ft of wall	(Compression)

Required Area of Reinforcing Steel:

Depth (d_2)	=	42.0 in	
xbar (from right)	=	23.6 in	
d_2 - xbar	=	18.4 in	
Ma = M_{wall} + P*(d_2-xbar)	=	575 k-ft / ft of wall	**Ma>1.2*Mcrack**
Design Moment (M_d)	=	**575** k-ft / ft of wall	
Reqr'd A_s = [M_d/(f_s*j*d_2) - P/(f_s)]	=	5.48 in^2 / ft of wall	
Actual A_s (per ft)	=	5.96 in^2 / ft of wall	**OK > reqr'd**

Note:
Due to a varying moment, # 9 bars spaced every 4-in are needed only at the top and bottom of diaphragm wall.
Please refer to Plaxis output for more information on the moment diagram of the diaphragm wall.

However, we still need to add the development length to the far-end of the reinforcing steel bars.

Development Length

# 9 Bars:	AASHTO 8.25		
$L_{d(basic)} = .04*A_b*fy/(f'c)^{1/2}$	=	37.7 in	
Factor	=	1.4	AASHTO 8.25.2
L_d (development length)	=	53 in	AASHTO 8.25.4
Lap Splices:	AASHTO 8.32.3		
$L_{d(basic)} = .04*A_b*fy/(f'c)^{1/2}$	=	37.7 in	
Factor	=	1.3	AASHTO 8.32.3.1
L_d (development length)	=	50 in	
Standard Hooks:	AASHTO 8.29		
$L_{hb} = 1200*d_b/(f'_c)^{1/2}$	=	21.3 in	
90-deg Hooks:			
Factor	=	0.7	AASHTO 8.29.3.4
L_{dh} (development length)	=	15 in	**OK**
Length of hook ($12*d_b$)	=	13.5 in	

Conclusion

From the previous analysis transverse reinforcing steel bars should be placed in the following manner:

a) For the entire depth of the wall use # 14 bars spaced every 4-in on the near-end of the wall to resist positive bending moments.

b) For the first 62 ft of wall depth, use # 9 bars spaced every 4-in on the far-end of the wall to resist negative bending moments.

c) For the last 70 ft of wall depth, use again # 9 bars spaced every 4-in on the far-end of the wall to resist negative bending moments.

Appendix F: Proposed Design for the Strutting System

Strutting System Design

Notes and Assumptions:
English System was adopted for these calcualtions. Converted values to Metric System are shown in thesis

Axial Loads: (Obtained from Plaxis output)

Strut	1	2	3	4	5	6	7	8	9	10
Pre-load Force	200	550	650	600	700	700	800	850	800	700
Phase 1	0	0	0	0	0	0	0	0	0	0
Phase 2	0	0	0	0	0	0	0	0	0	0
Phase 3	0	0	0	0	0	0	0	0	0	0
Phase 4	0	0	0	0	0	0	0	0	0	0
Phase 5	200	0	0	0	0	0	0	0	0	0
Phase 6	461	0	0	0	0	0	0	0	0	0
Phase 7	73	550	0	0	0	0	0	0	0	0
Phase 8	147	848	0	0	0	0	0	0	0	0
Phase 9	83	610	650	0	0	0	0	0	0	0
Phase 10	256	516	1419	0	0	0	0	0	0	0
Phase 11	178	510	893	600	0	0	0	0	0	0
Phase 12	264	367	924	1391	0	0	0	0	0	0
Phase 13	216	810	422	891	700	0	0	0	0	0
Phase 14	232	356	661	960	1481	0	0	0	0	0
Phase 15	218	389	689	836	1018	700	0	0	0	0
Phase 16	215	368	572	714	1138	1549	0	0	0	0
Phase 17	214	382	619	725	986	1063	800	0	0	0
Phase 18	208	388	591	644	878	1094	1670	0	0	0
Phase 19	211	388	612	681	898	1004	1115	850	0	0
Phase 20	211	390	612	663	849	934	1107	1486	0	0
Phase 21	212	388	614	677	877	958	1036	973	800	0
Phase 22	209	395	624	674	844	883	918	1230	2020	0
Phase 23	210	394	624	679	858	907	942	1100	1592	700
Phase 24	208	395	626	681	855	890	883	1037	1752	1142
MAX Values (KN/m)	**461**	**848**	**1419**	**1391**	**1481**	**1549**	**1670**	**1486**	**2020**	**1142**

Buckling Check: As per AISC Allowable Stress Design Standards

	1	2	3	(1*2+3)	
Strut Layer	Max Strut Reaction (KN/m)	Trib. Width (m)	Temp. Effect (KN/nos)	Design Forces	Pa = Design Forces (kips)
1	461	4.0	137	1981	445
2	848	2.0	97.2	1793.2	403
3	1419	2.0	59.9	2897.9	651
4	1391	2.0	58.8	2840.8	639
5	1481	2.0	54.5	3016.5	678
6	1549	2.0	50.6	3148.6	708
7	1670	2.0	102	3442	774
8	1486	2.0	103	3075	691
9	2020	2.0	97.1	4137.1	930
10	1142	2.0	103	2387	537

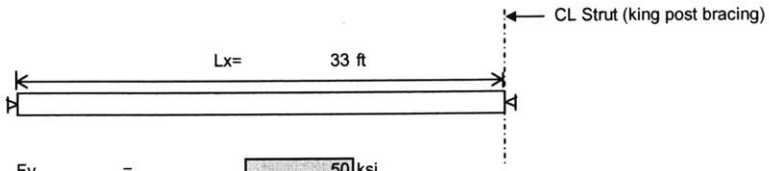

Fy	=	50	ksi
K	=	1.0	
Lx	=	33	ft
Ly	=	18	ft

ASD 5-135

ASD Table C-50
[using MAX(KLx/rx,Kly/ry)]

Strut	Section	rx (in)	ry (in)	KLx/rx	KLy/ry	Area (in^2)	Pa (kips)	fa (ksi)	Fa (ksi)	fa/Fa
1	W14x132	6.28	3.76	63	58	38.8	445	11.5	22.2	0.52
2	W14x132	6.28	3.76	63	58	38.8	403	10.4	22.2	0.47
3	W14x159	6.40	4.00	62	54	46.7	651	14.0	22.4	0.62
4	W14x159	6.40	4.00	62	54	46.7	639	13.7	22.4	0.61
5	W14x176	6.43	4.02	62	54	51.8	678	13.1	22.4	0.59
6	W14x176	6.43	4.02	62	54	51.8	708	13.7	22.4	0.61
7	W14x193	6.48	4.05	61	53	56.8	774	13.6	22.6	0.60
8	W14x176	6.43	4.02	62	54	51.8	691	13.3	22.4	0.60
9	W14x233	6.64	4.10	60	53	68.5	930	13.6	22.7	0.60
10	W14x145	6.33	3.98	63	54	42.7	537	12.6	22.2	0.57

Summary Table in Metric System

Strut	Section	Design Forces (KN)	Axial Capacities (KN)
1	W14x132	1981.0	3831.5
2	W14x132	1793.2	3831.5
3	W14x159	2897.9	4647.0
4	W14x159	2840.8	4647.0
5	W14x176	3016.5	5154.4
6	W14x176	3148.6	5154.4
7	W14x193	3442.0	5697.5
8	W14x176	3075.0	5154.4
9	W14x233	4137.1	6922.9
10	W14x145	2387.0	4216.6

Appendix G: Proposed Design for the Waler Connection

Waler Connection Design

Notes and Assumptions:
English System was adopted for these calcualtions. Converted values to Metric System are shown in thesis
Calculations done as per AASHTO Standards
Steel waler beams are the same size as the largest connecting strut

High strut reaction force (P) will cause waler beam web to sway (see figure below):

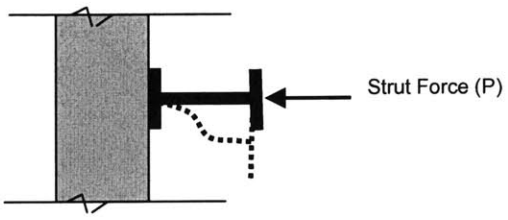

Waler Beam Cross-Section
NTS

To prevent this failure stiffner plates need to be incorporated:

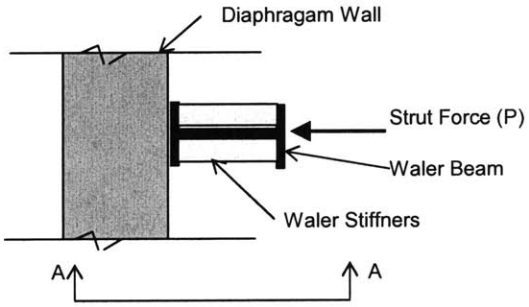

Wall Elevation
NTS

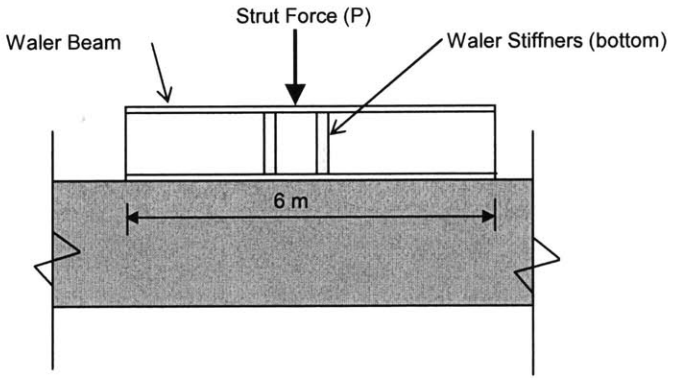

Section A-A
NTS

Waler Stiffners Design AASHTO 10.34.6 (Bearing Stiffners)

Max. Strut Force (P)	=	930 kips	(4137.1KN)

Waler beam properties:

Yield Strength (Fy)	=	50 ksi	
Length of Waler Beam	=	19.7 ft	(6m)
Waler Beam Size	=	W14x233	
Beam Depth (D)	=	16.04 in	
Flange width (b_f)	=	15.89 in	
Flange thickness (t_f)	=	1.72 in	
Web thickness (t_w)	=	1.07 in	
Stiffner spacing (do)	=	12 in	**OK < 1.5*D**
Strip of web (b)	=	31 in	

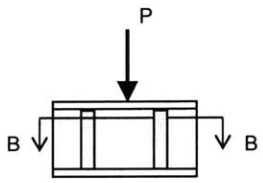

Waler Beam Elevation
NTS

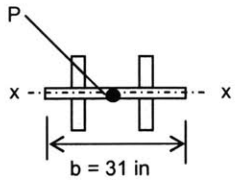

Section B-B
NTS

Check for buckling of stiffner plate:

Thickness of stiffner	=	1 in	**OK > 0.76 in**
Width of stiffner (w)	=	7.41 in	
Length of sitiffner (L)	=	12.6 in	
Moment of Inertia (Ix)	=	138.8 in^4	
Bearing Area (A_b)	=	63.1 in^2	
Radius of gyration (rx)	=	1.48 in	
Allowable Stress (Fa)	=	23.5 ksi	AASHTO Table 10.32.1A
Actual Stress (fa) = P/A_b	=	14.7 ksi	**OK < Fa**

Appendix H: Cost Analysis

Cost Analysis

The following are the cost increments associated with the proposed design:

Notes and Assumptions:

1. For practicality, only the increments of the costs associated with the diaphragm wall are included, since the changes made to the design of the strutting system should not have a strong impact on the cost of the original design.

2. Unit costs include all fringe benefits, taxes and insurance on labor (35%), general conditions and equipment (10%), and sales tax (5%).

3. Unit costs are the standar used in the US. It was assumed that these costs should not vary significantly in Singapore

Excavation Cost

Fill

Depth	=	4.7 m		
Length	=	33 m		
Thickness	=	0.4 m	(increased thickness of the diaphragm wall)	
Total Volume	=	62.04 m^3	=	81 CuYd
		Price per CuYd	=	$35.9
		Total Cost	=	**$2,915**

Estuarine Clay (Soft Clay)

Depth	=	1.8 m		
Length	=	33 m		
Thickness	=	0.4 m		
Total Volume	=	23.76 m^3	=	31 CuYd
		Price per CuYd	=	$45.8
		Total Cost	=	**$1,424**

Marine Clay (Upper and Lower - Soft Clay)

Depth	=	31 m		
Length	=	33 m		
Thickness	=	0.4 m		
Total Volume	=	409.2 m^3	=	535 CuYd
		Price per CuYd	=	$45.8
		Total Cost	=	**$24,532**

Fluvial Clay (Firm Clay)

Depth	=	3.8 m		
Length	=	33 m		
Thickness	=	0.4 m		
Total Volume	=	50.16 m^3	=	66 CuYd
		Price per CuYd	=	$64.3
		Total Cost	=	**$4,217**

Old Alluvium- SW2 (Hard - Sands & Clays)

Depth	=	3 m		
Length	=	33 m		
Thickness	=	0.4 m		
Total Volume	=	39.6 m^3	=	52 CuYd
		Price per CuYd	=	$74.4
		Total Cost	=	**$3,855**
		Total Excavation Cost	=	**$36,943**
		Mobilization Factor	=	5%
		Total Cost for Excavation & Mobilization	=	**$38,790**

Material Costs

Concrete:

Wall Depth	=	44.3 m		
Wall Length	=	33 m		
△ Thickness	=	0.4 m	(increased thickness of the diaphragm wall)	
Total Volume	=	584.76 m^3	=	765 CuYd
		Price per CuYd	=	$110.4
		Total Cost for Concrete	=	**$84,465**

Reinforcing Steel Bars:

Positive Moment (near-end)

Original Design (Please refer to Appendix A)			*Revised Design*			
Area of Steel	=	0.33614209 m^2	Area of Steel	=	0.056977 m^2/m	= 26.92 in^2/ft
Rebar Depth	*(already included in area of steel)*		Rebar Depth	=	44.3 m	
Wall Length	=	33 m	Wall Length	=	33 m	
Total Volume	=	11.09 m^3	Total Volume	=	83.29 m^3	
	=	15 CuYd		=	109 CuYd	

Negative Moment (far-end)

Original Design (Please refer to Appendix A)			*Revised Design*			
Area of Steel	=	0.275622257 m^2	Area of Steel	=	0.012624 m^2/m	= 5.96 in^2/ft
Rebar Depth	*(already included in area of steel)*		Rebar Depth	=	39.9 m	
Wall Length	=	33 m	Wall Length	=	33 m	
Total Volume	=	9.10 m^3	Total Volume	=	16.63 m^3	
	=	12 CuYd		=	22 CuYd	

Total Rebar Volume in *Original* Design	=	26 CuYd
Total Rebar Volume in *Revised* Design	=	131 CuYd
Volume Difference *(Revised - Original)*	=	104 CuYd
Specific Weight of Steel	=	6.615 Tons/CuYd
Total Increased Steel Rebar Weight	=	**690 Tons**
Price per Ton	=	$2,027
Total Cost for Steel Reinforcement	=	**$1,398,465**

Summary of Cost Increment with Proposed Design

Total Cost for Excavation & Mobilization	=	$38,790
Total Cost for Concrete	=	$84,465
Total Cost for Steel Reinforcement	=	$1,398,465
Cost Increment (per excavation side)	=	$1,521,720
Cost Increment under Revised Design	=	**$3,043,439**